

Thermodynamic assessment of the Ba–La–S and Ga–La–S systems

Jiayang Wang^a, Guangyu Hu^a, Pierre Lucas^a, Marat I. Latypov^{a,b,*}

^a*Department of Materials Science and Engineering, University of Arizona, Tucson, AZ 85721, USA*

^b*Graduate Interdisciplinary Program in Applied Mathematics, University of Arizona, Tucson, AZ 85721, USA*

Abstract

This paper presents the first thermodynamic assessment of binary and pseudo-binary phase diagrams in the Ba–La–S and Ga–La–S systems by means of the CALPHAD method. Experimental phase diagram equilibrium data and thermodynamic properties available from the literature were critically reviewed and assessed using thermodynamic models for the Gibbs energies of individual phases. The associated solution model was used to describe the short-range ordering behavior of the liquid phases. To supplement the limited experimental data reported in the literature, ab initio molecular dynamics calculations were employed to derive mixing enthalpies of the liquid phases in the binary subsystems. The resulting phase diagrams and calculated thermodynamic properties show good agreement with available literature within the investigated compositional ranges of binary and pseudo-binary systems.

Keywords: Chalcogenides, phase diagrams, thermodynamic assessment, CALPHAD, Ab-initio calculations

1. Introduction

Refractory rare-earth sulfide materials are of increasing interest for applications in infrared (IR) optics, semiconductor devices, and protective coatings [1, 2] thanks to their excellent combination of mechanical, thermal, and optical properties [2, 3]. For example, high melting points of such sulfide compounds as BaS ($T_m = 2454$ K) [4], La₂S₃ ($T_m = 2211$ K) [5], and Ga₂S₃ ($T_m = 1393$ K) [6] make them promising candidates for high temperature applications. Nevertheless, rare-earth sulfides remain an emerging materials class with significantly fewer studies to date compared to more established systems such as oxide-based materials [7].

*corresponding author

Email address: latmarat@arizona.edu (Marat I. Latypov)

Supporting further development and deployment of rare-earth sulfides requires a deep understanding of their phase stability and thermodynamic behavior. Most of the published knowledge on phase equilibria and thermodynamic properties of these materials is based on direct experimental observations with a noticeable lack of thermodynamic models developed with the modern computational approaches, such as the CALPHAD (CALculation of PHAse Diagrams) method [8]. Reliance solely on experiments hinders efficient exploration of the compositional design space in pursuit of advanced performance. In this context, the development of computational thermodynamic models are essential for guiding targeted synthesis and processing as well as for predicting properties without extensive experimentation.

This work aims to fill this gap for two sulfide systems: La–Ba–S and La–Ga–S, both of which have strong potential for advanced applications offering high thermal stability with broad IR transparency and glass-forming ability [9, 10]. Specifically, we establish a thermodynamic database that contains thermodynamic models for all experimentally observed phases calibrated to experimental and computational data available in the literature. We further supplemented literature data with thermodynamic property data from ab initio molecular dynamics (AIMD) simulations of liquid phases, for which published information is very limited. To this end, we first review the literature for the relevant binary and ternary systems and summarize the phases considered for the thermodynamic assessment in this study (Section 2). We then describe the thermodynamic models adopted for the phases, fit the corresponding parameters to the compiled literature data (Section 3.2) and our AIMD results (Section 4.1). Finally, we compare the calculated phase diagrams and thermodynamic properties with both experimental and simulation data for these systems (Section 4.2). Given a limited scope of published data on the systems of interest, we focus on binary and pseudo-binary phase diagrams in this study.

2. Literature review

The CALPHAD method is a hierarchical and self-consistent framework for developing thermodynamic models of multicomponent systems [11]. In line with the CALPHAD approach, this section reviews experimental data that are directly relevant to the two systems examined in this study. Specifically, we cover all the binary systems (Ba–S, Ba–La, La–S, Ga–S) except Ga–La, for which a thermodynamic description is already available from Boudra et al. [12]. Tables 1 and 2 summarize all the phases (and their crystal structures) in the Ba–La–S and Ga–La–S systems considered in this study as a result of the literature review detailed below.

2.1. Phase diagram data

Barium–Sulfur. The Ba–S phase diagram has been reported for a limited composition range between 50 and 80 at.% of sulfur by Robinson et al. [13], who used thermal analysis. This restriction arises because, at the high temperatures

required to investigate Ba-rich and S-rich alloys, containing sulfur vapor in sealed vessels is extremely challenging: sulfur is highly reactive with refractory container materials, making it difficult to maintain a fixed overall composition during equilibration and thus limiting the experimentally accessible portion of the diagram [14, 15]. Within this accessible range, Robinson et al. identified several invariant reactions by thermal arrest measurements, including the melting temperature of high-temperature phase ht-BaS₂ (1198 K), the phase transition from ht-BaS₂ to lt-BaS₂ at 973 K, and the melting temperature of BaS₃ (827 K) [13]. The ht-BaS₂ to lt-BaS₂ transition was later confirmed by Kawada et al. [16]. For BaS, early structural studies date back to 1923, when Holgersson [17] determined its crystal structure by X-ray diffraction (XRD), later refined by Güntert and Faessler [18]. More recent work reported the melting point of BaS as 2454 K [4], 2470 K [19], and 2480 K [20]. Because BaS is highly volatile near 2500 K, small differences in sulfur vapor pressure control, sample purity, and measurement method vary the reported melting point. Metastable Ba₂S₃ (studied by Yamaoka et al. [21]) forms only under high-pressure conditions and is absent from the phase diagram at ambient pressure. Regarding the liquidus, Robinson et al. [13] reported only a single data point between BaS and BaS₂. Between BaS₂ and BaS₃, they observed a sharp liquidus drop of 350 °C for just a 4 % change in composition, whereas, beyond BaS₃, the liquidus line flattens considerably. As liquidus data are scarce, it remains unclear whether the melting of ht-BaS₂ and BaS₃ is congruent or incongruent. Robinson et al. speculated a eutectic reaction based on extrapolation. In this work, we fit the liquidus line accordingly and model eutectic melting behavior of the compounds.

Barium–Lanthanum. The Ba–La phase diagram has received little attention, with the only experimental investigation conducted by Pyagai et al. [22]. Their phase diagram indicates solid solutions in both Ba- and La-rich composition ranges, with about 0.2 at.% solubility of La in Ba and 1 at.% of Ba in La. The limited solubility indicates positive enthalpy of mixing between Ba and La atoms in the solid phases (b.c.c.-Ba, b.c.c.-La and f.c.c.-La). Below the melting point, the phase diagram is dominated by two-phase regions with no intermetallic compounds. At elevated temperatures above the melting point, a large miscibility gap spans a broad compositional range from approximately 0.4 to 90 at.% of La.

Lanthanum–Sulfur. The La–S phase diagram was experimentally investigated by Kamarzin et al. [5] and Mironov et al. [23] through visual polythermal method and high-temperature annealing. Based on these studies, Massalski et al. [6] assessed and constructed a La–S phase diagram for concentrations of sulfur below 70 at.%. At higher sulfur contents, the vapor pressure of sulfur becomes too high to maintain a well-defined bulk composition during equilibration, preventing reliable phase-diagram measurements in a manner analogous to the Ba–S system. The La–S binary system contains the LaS single phase and La₂S₃ polymorphic phases. Westerholt et al. [24] experimentally determined the crystal structure and lattice parameter of LaS, while other researchers measured its congruent melting point as approximately 2573 K [5, 25]. For La₂S₃, three polymorphs (α , β , and γ) have been reported. The polymorph α -La₂S₃ adopts

a Gd_2S_3 -type orthorhombic structure and belongs to the $Pnam$ space group [26]. The α polymorph is stable at low temperatures and undergoes an irreversible transformation to $\beta\text{-La}_2\text{S}_3$ at $650\pm50\text{ }^\circ\text{C}$ [27]. The tetragonal $\beta\text{-La}_2\text{S}_3$ with the $I4_1/acd$ space group is stabilized as an oxysulfide that replaces some sulfur atoms with oxygen, forming compositions $\text{La}_{10}\text{S}_{15-x}\text{O}_x$, $0 \leq x \leq 1$ [28]. In this structure, each La atom is surrounded by eight S atoms in a dodecahedral arrangement with dodecahedra sharing triangular faces or edges with neighboring units. The transformation from $\beta\text{-La}_2\text{S}_3$ to $\gamma\text{-La}_2\text{S}_3$ occurs at temperatures up to $1300\text{ }^\circ\text{C}$ [29]. The $\gamma\text{-La}_2\text{S}_3$ polymorph is a solid solution adopting a cubic Th_3P_4 -type structure in the $I\bar{4}3d$ space group with a stoichiometric composition $\text{La}_{3-x}\text{Va}_x\text{S}_4$ ($0 \leq x \leq 1/3$), where Va denotes vacancies in the lanthanum sublattice, spanning compositions between La_2S_3 and La_3S_4 . The melting point decreases with composition from La_3S_4 to La_2S_3 [5]. The melting point of La_3S_4 was reported as 2383 K [5], while La_2S_3 has been reported (by multiple groups [5, 30, 31]) to melt in a range between 2133 and 2211 K . The potential reactivity with crucibles might have affected the accuracy of the results [4]. Kamarzin et al. additionally include two eutectic points in the phase diagram: one between LaS and La_2S_3 at 1985 K at 54.6 at.% of sulfur, another one at 1191 K and 0.01 at.% of sulfur [5]. LaS_2 polymorphs were reported by Dugue et al. (orthorhombic, $Pna2_1$) and Le Rolland et al. (monoclinic, $P12_1/c1$) [32, 33], with a melting temperature of 1917 K .

| Phase | Prototype | Pearson symbol | Space group | Description |
|--------------------------------|---------------------------------|----------------|--------------|---|
| b.c.c-Ba | Ba | cI2 | $Im\bar{3}m$ | Solid soln. in b.c.c Ba |
| d.h.c.p-La | $\alpha\text{-La}$ | hP4 | $P6_3/mmc$ | d.h.c.p La |
| f.c.c-La | W | cI2 | $Im\bar{3}m$ | Solid soln. in f.c.c La |
| b.c.c-La | Cu | cF4 | $Fm\bar{3}m$ | Solid soln. in b.c.c La |
| S | $\alpha\text{-S}$ | oF128 | $Fddd$ | - |
| BaS | NaCl | cF8 | $Fm\bar{3}m$ | Binary phase BaS |
| lt-BaS ₂ | BaS ₂ | mS16 | $C2/c$ | Binary phase BaS ₂ |
| ht-BaS ₂ | CaC ₂ | tI6 | $I4/mmm$ | Binary phase BaS ₂ |
| BaS ₃ | BaS ₃ | tP8 | $P4_21m$ | Binary phase BaS ₃ |
| LaS | NaCl | cF8 | $Fm\bar{3}m$ | Binary phase LaS |
| $\alpha\text{-La}_2\text{S}_3$ | Gd ₂ S ₃ | oP40 | $Pnam$ | Binary phase La ₂ S ₃ |
| $\beta\text{-La}_2\text{S}_3$ | Ca ₂ Si ₃ | tI80 | $I4_1/acd$ | Binary phase La ₂ S ₃ |
| $\gamma\text{-La}_2\text{S}_3$ | Th ₃ P ₄ | cI28 | $I\bar{4}3d$ | Solid soln. in cubic La ₂ S ₃ |
| LaS ₂ | - | - | - | Binary phase LaS ₂ |

Table 1: Phases in the Ba–La–S system considered in this study and their symbols.

Gallium–Sulfur. The experimental phase diagram of the Ga–S system remains unsettled. The discrepancies among the reported phase diagrams arise from experimental challenges. Specifically, the low volatility of gallium chalcogenides at sulfur mole fractions below 0.6 complicates vapor pressure measurements and impedes the growth of single crystals with uniform composition. The

ambiguity of electrical measurements further contributes to inconsistencies in the reported data [34]. Below, we outline the two prevailing interpretations of the phase diagram found in the literature.

Rustanov et al. [35] investigated the system in the sulfur composition range up to 60 at.%, and their findings were summarized in a phase diagram by Masałski et al. [6]. This phase diagram includes a narrow liquid–liquid miscibility gap between 2 and 17 at.% sulfur at 1208 K as well as solid phases GaS, Ga₂S, Ga₂S₃, and Ga₄S₅. The phases GaS and Ga₂S₃ have been confirmed by subsequent studies [36–38], whereas the phases Ga₂S and Ga₄S₅ described by Rustanov et al. as incongruently melting intermediate compounds are less established. Although Ga₄S₅ was independently observed [39], neither the existence nor the structure of Ga₂S or Ga₄S₅ has been confirmed by other reports [40]. Given these concerns, we do not consider the intermediate phases Ga₂S and Ga₄S₅ nor the liquid–liquid miscibility gap in the Ga-rich region proposed by Rustanov et al. [35].

Several studies proposed an alternative view of the Ga–S phase diagram for the full composition range [36–38, 41], which includes two distinct liquid–liquid miscibility gaps: one between Ga and GaS, and another between Ga₂S₃ and S. The Ga-rich miscibility gap at 1203 K spans a wide range from 10.3 to 48.4 at.% sulfur, a finding supported earlier by Spandau and Klanberg [39]. Lieth et al. [41] also noted that analogous immiscibility regions exist in similar systems such as Ga–Te [42], In–Te [43], and In–S [44], which suggests that the monotectic point on the Ga-rich side lies very close to pure Ga. The S-rich liquid–liquid miscibility gap was reported to extend from 70 to 95 at.% sulfur at 1266 K [36]. For the generally accepted phases GaS and Ga₂S₃, Pardo et al. [36] and Lieth et al. [41] reported consistent melting points of 1235 K for GaS and 1363 K for Ga₂S₃, both of which are lower than those reported by Rustanov et al. [35]. This study adopts the phase diagram of Pardo et al. and Lieth et al. owing to their better consistency and broader acceptance in the literature.

For GaS and Ga₂S₃, Zlomanov and Novoselova [37] suggested these phases represent primary stable compounds that form a eutectic system with a melting point above 1223 K. More recent studies by Zavrazhnov et al. [40] and Berezin et al. [45] investigated the high-temperature phase diagram in the 48 to 60.7 at.% sulfur range using differential thermal analysis (DTA) and chromatic–thermal analysis (CrTA). Their results showed that the system consists only of GaS and Ga₂S₃ at temperatures below 1151 K. A higher temperatures (1151 to 1383 K), the phase diagram becomes more complex with three distinct phases in a narrow compositional range (59 to 60.7 at.% sulfur): σ (Ga_{0.41}S_{0.59}), Ga₂S₃', and γ -Ga₂S₃ [40]. Although the structural details of the σ phase are unknown, it is a line compound with about 59 at.% S. This phase is stable only within a limited temperature range (1151 to 1195 K) and decomposes at 1195 K via a peritectic reaction $\sigma \rightleftharpoons L + \text{Ga}_2\text{S}_3'$. Two polymorphs of gallium sesquisulfide were also identified: a low-temperature monoclinic form (γ -Ga₂S₃) and a high-temperature wurtzite-type form (Ga₂S₃') [40]. These phases exhibit nearly identical compositions and coexist at elevated temperatures (near 1243 K), suggesting that Ga₂S₃' behaves as a solid solution. The following eutectic reaction

| Phase | Prototype | Pearson symbol | Space group | Description |
|---|--------------------------------|----------------|---------------------------|---|
| Ga | Ga | oS8 | <i>Cmca</i> | Orthorhombic Ga |
| GaS | GaS | hP8 | <i>P6₃/mmc</i> | Binary phase GaS |
| α -Ga ₂ S ₃ | wurtzite | mP80 | <i>Cc</i> | Binary phase α -Ga ₂ S ₃ |
| β -Ga ₂ S ₃ | β -wurtzite | hP4 | <i>P6₃mc</i> | Binary phase β -Ga ₂ S ₃ |
| γ -Ga ₂ S ₃ | sphalerite | cF40 | <i>F43m</i> | Binary phase γ -Ga ₂ S ₃ |
| σ | - | - | - | Binary phase σ |
| Ga ₂ S ₃ ' | wurtzite | hP24 | <i>P6₁</i> | Solid soln. in Ga ₂ S ₃ ' |
| LaGaS ₃ | La ₂ S ₃ | mP12 | <i>P2₁c</i> | Ternary phase LaGaS ₃ |
| La ₉ Ga ₅ S ₂₁ | | hR30 | <i>R3</i> | Ternary phase La ₉ Ga ₅ S ₂₁ |

Table 2: Phases in the Ga–La–S system considered in this study and their symbols. Phases for the Ga–La system, thermodynamically assessed elsewhere [12], are not shown.

occurs at 1184 K and 59.5 at.% sulfur: $\sigma + \gamma\text{-Ga}_2\text{S}_3 \rightleftharpoons \text{Ga}_2\text{S}_3'$. In addition, $\gamma\text{-Ga}_2\text{S}_3$ undergoes a peritectic decomposition at 1279 K: $\gamma\text{-Ga}_2\text{S}_3 \rightleftharpoons L + \text{Ga}_2\text{S}_3'$ [40]. At higher temperatures, Ga₂S₃' adopts a defective wurtzite structure in which sulfur atoms form a hexagonal close-packed arrangement. Gallium atoms occupy only two-thirds of the upward-oriented X_4 tetrahedral sites in an ordered manner. The presence of unoccupied sites in Ga₂S₃' provides the structural basis for its solid-solution behavior [46, 47].

Investigations of Ga₂S₃ below 1073 K revealed three polymorphs: α , β , and γ [6, 48–50]. The low-temperature α -Ga₂S₃ phase adopts a monoclinic crystal structure in the *Cc* space group with ordered vacancies [48–50]. The β -Ga₂S₃ phase is stable at intermediate temperatures [6], while the γ -Ga₂S₃ phase is observed at higher temperatures according to the phase diagram proposed by Massalski et al. [6]. However, the precise transition temperatures among the Ga₂S₃ polymorphs remain uncertain.

Barium–Lanthanum–Sulfur. Experimental data for the ternary Ba–La–S phase diagram are rather limited. Andreev et al. [51] conducted comprehensive research on BaS–Ln₂S₃, including BaS–La₂S₃ (Ln for Lanthanides). Using XRD, differential thermal analysis (DTA), and visual polythermal analysis, these authors found that the light lanthanide sulfides do not form intermediate compounds but have extensive solid solubilities of BaS. The solubility of BaS in Ln₂S₃ decreases as the atomic number of the lanthanide element increases. Recently, Boury and Allanore [4] investigated the pseudo-binary BaS–La₂S₃ system above 1573 K using high-resolution *in situ* imaging combined with thermal arrest measurements. The observation of melts in a container-free environment resulted in melting points of the BaS and La₂S₃ phases equal to 2454 and 2004 K, respectively. The researchers reported two eutectic points at 1790 K and 1805 K. However, such *in situ* imaging captures only the surface phenomena, which may not represent the bulk behavior, especially in the absence of support from direct characterization for phase identification. For this reason, we exclude these data [4] from further analysis in this study.

Gallium–Lanthanum–Sulfur. Most studies of the Ga–La–S system, focused on the pseudo-binary Ga_2S_3 – La_2S_3 section. Loireau et al. [10] measured solidus lines and invariant points, and identified two intermetallic compounds: LaGaS_3 , which melts incongruently at 1225 K, and $\text{La}_9\text{Ga}_5\text{S}_{21}$, which melts congruently at 1425 K. Bakhtiyarly et al. [52] examined the La_2S_3 – Ga_2S_3 – EuS ternary system using differential thermal analysis and XRD. Their results within the Ga_2S_3 – La_2S_3 subsystem confirmed several invariant reactions identified Loireau et al. [10]. Since no liquidus line was reported for this pseudo-binary system, we fit the liquidus line to invariant reactions, adopting the experimental phase diagram of Loireau et al. [10].

2.2. Thermodynamic data

2.2.1. Ba–S system

For the Ba–S system, most available studies focused on BaS , whose thermodynamic properties are summarized in the NIST-JANAF Thermochemical Tables [53], including heat capacity C_p , the Gibbs free energy of formation ΔG , the enthalpy increment $H(T) - H(298 \text{ K})$ and formation enthalpy $\Delta H(298\text{K})$. King and Weller [54] studied heat capacity of BaS at low temperatures and reported a room-temperature value of 49.374 J/mol K. Above 300 K, heat capacity values were extrapolated using graphical methods and Kubaschewski's method B [55]. Tuncel et al. [56] computed the thermodynamic properties of BaS using the density functional theory (DFT). The DFT results were confirmed by Rino et al. [57] using molecular dynamics (MD) simulations. Both computational studies agree with experiments near room temperature but deviate at elevated temperatures due to the neglect of anharmonic effects [58].

2.2.2. La–S system

For the La–S system, Bolgar et al. [59] measured heat capacity, entropy, and enthalpy increment of lanthanum sulfide compounds covering a range of La:S ratios using differential calorimetry. Vasilev et al. [60] examined the low-temperature physical properties of rare-earth monosulfides, including LaS , using a vacuum adiabatic calorimeter over a temperature range from 2 to 300 K. Their results for heat capacity are in good agreement with those of Bolgar et al. [59] at room temperature. The formation enthalpy of LaS have been investigated by Semenkovich et al. [61] using solution reaction calorimetry.

For compound $\gamma\text{-La}_2\text{S}_3$, besides the measurement by Bolgar et al. [59], Amano et al. [62] measured the heat capacity and enthalpy increment using a copper block drop calorimeter. Westrum et al. [63] further investigated the low-temperature entropy and heat capacity using adiabatic calorimetry. The results from these studies [59, 62, 63] are consistent within the overlapping temperature ranges. More recently, Vasilyeva and Nikolaev [64] measured the heat capacity and formation enthalpy using a sensitive static tensimetric method at room temperature and their heat capacity deviated about 1.6 % from previous results [59, 63].

For La_3S_4 , Amano et al. [62] reported the heat capacity and enthalpy increment. Compared to Bolgar et al. [59], their heat capacity values differ by 4 %

at room temperature, whereas the enthalpy increment is consistent. Viennois et al. [65] obtained formation enthalpy and heat capacity at room temperature with the latter in agreement with values from Bolgar et al. [59] within 0.3 %.

For LaS_2 , experimental data are scarce with the only reports of heat capacity provided by Vasilyeva and Nikolaev [64] and Bolgar et al. [59], who additionally measured enthalpy increment for the phase.

2.2.3. *Ga–S system*

An early estimation of the heat capacity of Ga_2S_3 was provided by Moiseev and Sesták [66] using the Neumann–Kopp rule. More recently, Rika et al. [67] performed a comprehensive experimental and computational investigation on heat capacity and entropy of Ga_2S_3 . The authors used two techniques for low- and high-temperature measurements: relaxation calorimetry from 2 to 302 K and Tian–Calvet calorimetry in the range 271 to 1252 K. They supported these measurements with DFT calculations of the heat capacity that showed good agreement with the experiment. Rika et al. [67] also reported entropy in the temperature range from 0 to 350 K and room temperature formation enthalpy based on DFT. Barin & Platzki [68] reported the formation enthalpy of Ga_2S_3 at room temperature using solution calorimetric measurements.

For GaS , Sedmidubský et al. [69] reported the heat capacity over a wide range of temperatures using calorimetric measurements supplemented by theoretical modeling of both heat capacity and formation enthalpy using the Debye–Einstein approach. Two devices over different temperature range were employed: physical property measurement system (PPMS) Evercool-II equipment from 2 to 300 K and Micro DSC–III calorimeter from 258 to 358 K. They also provided heat capacity and formation enthalpy with theoretical modeling based on the Debye–Einstein approach. Hahn et al. [70] also reported the room temperature formation enthalpy of GaS .

3. Methods

3.1. *Ab initio molecular dynamics*

To obtain thermodynamic properties of the liquid phases with scarce experimental data, we performed AIMD simulations within the framework of density functional theory (DFT) using the Vienna Ab initio Simulation Package (VASP) [71]. The electronic wave functions were expanded in a plane-wave basis set under periodic boundary conditions [72], with a plane-wave cutoff energy of 400 eV. The exchange–correlation functional was described by the generalized gradient approximation [73]. The projector augmented wave method was used to describe the interaction between valence electrons and ion cores [74]. Brillouin zone sampling was restricted to the Γ -point. All simulations were carried out in the canonical NVT ensemble with the temperature controlled by a Nosé–Hoover thermostat [75, 76]. Newtons equations of motion were integrated using the Verlet algorithm with a time step of 2 fs. The final 1000 configurations were used to statistically evaluate the thermodynamic and structural properties.

Thermodynamic properties were calculated for the Ba–La, La–LaS, and Ga–GaS liquids. BaS and the sulfur-rich regions of the La–S and Ga–S systems were not considered because, at the temperatures of interest, the pure components are volatile: BaS melts near 2500 K [4], well above the boiling point of Ba (2118 K at 1 atm) [77], while sulfur boils at 718 K [77]. The simulations analyzed Ba–La and Ga–GaS at 1600 K and La–LaS at 3200 K. These temperatures were selected above the melting points and below the boiling points of relevant phases to ensure the evaluation of their liquid state. All supercells were constructed as cubic cells containing 128 atoms. The mixture compositions were specified at atomic fraction $\{0.2, 0.4, 0.5, 0.6, 0.8\}$, along with pure reference states. The supercell volumes were fine-tuned to maintain the external pressure within ± 5 kbar, thereby minimizing the influence of pressure on the structure and total energy of the systems. To confirm that the chosen temperature was sufficient for melting and that the simulation time was long enough to reach equilibrium, pair correlation functions (PCFs) were calculated at selected stable time steps. The mixing enthalpy ΔH_{mix} was calculated as follows (taking the Ba–La system as an example):

$$\Delta H_{\text{mix}} = \frac{E_{\text{mix}} - N_{\text{Ba}} \cdot E_{\text{Ba}} - N_{\text{Ga}} \cdot E_{\text{Ga}}}{N_{\text{Ba}} + N_{\text{Ga}}}, \quad (1)$$

where E_{mix} is the average energy of the mixture supercell, N_{Ba} and N_{Ga} are the numbers of Ba and Ga atoms in the supercell, and E_{Ba} and E_{Ga} are the energies of pure Ba and pure Ga per atom, respectively.

3.2. Thermodynamic modeling

For the pure elements (Ga, Ba, La, and S), we adopted the Gibbs free energy functions from the SGTE database [78]. For the binary and ternary phases, we selected appropriate models that describe substitutional solutions, stoichiometric compounds, liquid phases with short-range order, and solid phases with vacancies and substitutions. These models and their calibration to the experimental data (reviewed in Section 2) are described below.

3.2.1. Substitutional solutions

For all liquid phases as well as solid b.c.c.-Ba, f.c.c.-La, and b.c.c.-La phases, we adopted a substitutional solution model suitable for random (liquid and solid) solutions. This model describes the molar Gibbs free energy, G^ϕ , of a solution phase ϕ using the Redlich–Kister–Muggianu polynomial [79]. For the b.c.c. system as an example:

$$\begin{aligned} G^{\text{b.c.c.}} = & \sum_{i=\text{Ba,La}} x_i^\circ G_i^{\text{b.c.c.}} + RT \sum_{i=\text{Ba,La}} x_i \ln(x_i) \\ & + x_{\text{Ba}} x_{\text{La}} \sum_{\theta=0} L_{\text{Ba,La}}^{\text{b.c.c.}} (x_{\text{Ba}} - x_{\text{La}})^\theta, \end{aligned} \quad (2)$$

where x_i denotes the molar fraction, ${}^\circ G_i^{\text{b.c.c.}}$ denotes the Gibbs free energy in the reference state of the b.c.c. phase, R is the gas constant, T is the temperature in Kelvin. The interaction parameters, ${}^\theta L_{\text{Ba},\text{La}}^{\text{b.c.c.}}$ ($\theta \in [0, 4]$), are considered to linearly depend on temperature: ${}^\theta L_{\text{Ba},\text{La}}^{\text{b.c.c.}} = {}^\theta A_{\text{Ba},\text{La}}^{\text{b.c.c.}} + {}^\theta B_{\text{Ba},\text{La}}^{\text{b.c.c.}} \cdot T$. The parameters ${}^\theta A_{\text{Ba},\text{La}}^{\text{b.c.c.}}$ and ${}^\theta B_{\text{Ba},\text{La}}^{\text{b.c.c.}}$ shall be calibrated to the experimental data.

3.2.2. Stoichiometric compounds

The Ba–S, La–S, and Ga–S binary systems include stable stoichiometric compounds (such as BaS, BaS₂, BaS₃, LaS, GaS, Ga₂S₃). For the compounds that lack published thermodynamic information, we estimate the molar Gibbs free energies using the Neumann–Kopp rule [80–82]:

$$G_f^{M_x N_y} = x \cdot {}^\circ G_M + y \cdot {}^\circ G_N + A_{M_x N_y} + B_{M_x N_y} \cdot T, \quad (3)$$

where x and y are the stoichiometric coefficients and $A_{M_x N_y}$ and $B_{M_x N_y}$ are the adjustable parameters for compounds $M_x N_y$. For the compounds with available experimental heat capacity data, higher order parameters are included to describe the deviation from Neumann–Kopp rule of the measured heat capacity:

$$G_f^{M_x N_y} = x \cdot {}^\circ G_M + y \cdot {}^\circ G_N + A_{M_x N_y} + B_{M_x N_y} \cdot T + C_{M_x N_y} \cdot T \cdot \ln(T) + D_{M_x N_y} \cdot T^{-1} + E_{M_x N_y} \cdot T^2, \quad (4)$$

3.2.3. Liquid phases with short-range order

In the Ba–S, La–S, and Ga–S binary phase diagrams, the melting points of compounds are much higher than those of the corresponding pure elements. We therefore assume that, in the liquid phase, the compounds retain strong attractive interactions even at temperatures higher than their melting points. Consequently, short-range chemical order is likely to occur in the liquid state [83]. The associated solution model was chosen for the BaS, LaS, La₂S₃, GaS, and Ga₂S₃ phases. As a specific example, the Gibbs energy of La₂S₃ in the liquid state is written as:

$$G^{\text{Liq}} = \sum_i x_i G_i^{\text{Liq}} + RT \sum_i x_i \ln(x_i) + G_{\text{exc}}^{\text{Liq}}, \quad (5)$$

where x_i is the mole fraction of the i^{th} species ($i \in \{\text{La, S, La}_2\text{S}_3\}$) in the liquid phase and $G_{\text{exc}}^{\text{Liq}}$ is the excess Gibbs free energy expressed as:

$$G_{\text{exc}}^{\text{Liq}} = \sum_i \sum_{j \neq i} x_i x_j \sum_{\theta=0}^n {}^\theta L_{i,j}^{\text{Liq}} (x_i - x_j)^\theta \quad (6)$$

with $i, j \in \{\text{La, S, La}_2\text{S}_3\}$. The binary interaction parameters are linear functions of temperature ${}^\theta L_{i,j}^{\text{Liq}} = {}^\theta A_{i,j}^{\text{Liq}} + {}^\theta B_{i,j}^{\text{Liq}} \cdot T$, the parameters ${}^\theta A_{i,j}^{\text{Liq}}$ and ${}^\theta B_{i,j}^{\text{Liq}}$ are to be calibrated.

3.2.4. Solid solution phase with vacancies and substitution

Based on literature sources [4, 5, 84], the non-stoichiometry of the γ -La₂S₃ phase arises from the presence of vacancies on the La sublattice. The actual composition, accounting for vacancies (V_a), is expressed as γ -La_{2.25-x}V_xS₃, where $0 \leq x \leq 0.25$. This range corresponds to the end-members γ -La_{2.25}S₃ (La₃S₄) and γ -La₂S₃. To describe the γ -La₂S₃ phase considering vacancies, the sublattice model can be (La)₂(La, V_a)_{0.25}(S)₃. For the Ba-La-S ternary system, literature data [51] report approximately 50 % solid solubility of BaS in γ -La₂S₃, resulting in the formation of an intermediate phase with an approximate composition of Ba_{0.75}La_{1.5}S₃ (BaLa₂S₄). Although the detailed substitution mechanism is not specified, it is assumed that partial substitution of La by Ba accounts for the observed composition. Accordingly, the sublattice model used in the Ba-La-S database for this phase is (La)_{1.25}(La, Ba)_{0.75}(La, V_a)_{0.25}(S)₃. In contrast, for the Ga-La-S ternary system, no significant solubility of γ -La₂S₃ in the Ga₂S₃-La₂S₃ pseudo-binary system has been reported. Therefore, the original sublattice model (La)₂(La, V_a)_{0.25}(S)₃ is retained for γ -La₂S₃ in this system. For Ba-La-S system, the three terms of the γ -La₂S₃ Gibbs energy functions are:

$$G_{\text{ref}}^{\gamma-\text{La}_2\text{S}_3} = y'_{\text{La}} y''_{V_a} G_{\text{La:La:V}_a:\text{S}}^{\gamma-\text{La}_2\text{S}_3} + y'_{\text{La}} y''_{\text{La}} G_{\text{La:La:La:S}}^{\gamma-\text{La}_2\text{S}_3} + y'_{\text{Ba}} y''_{V_a} G_{\text{La:Ba:V}_a:\text{S}}^{\gamma-\text{La}_2\text{S}_3} + y'_{\text{Ba}} y''_{\text{La}} G_{\text{La:Ba:La:S}}^{\gamma-\text{La}_2\text{S}_3}, \quad (7a)$$

$$G_{\text{ide}}^{\gamma-\text{La}_2\text{S}_3} = RT[0.75(y'_{\text{La}} \ln(y'_{\text{La}}) + y'_{\text{Ba}} \ln(y'_{\text{Ba}})) + 0.25(y''_{\text{La}} \ln(y''_{\text{La}}) + y''_{V_a} \ln(y''_{V_a}))], \quad (7b)$$

$$G_{\text{exc}}^{\gamma-\text{La}_2\text{S}_3} = y'_{\text{La}} y'_{\text{Ba}} y''_{\text{La}} \sum_{\theta=0}^n \theta L_{\text{La:La,Ba:La:S}}^{\gamma-\text{La}_2\text{S}_3} (y'_{\text{La}} - y'_{\text{Ba}})^\theta + y'_{\text{La}} y'_{\text{Ba}} y''_{V_a} \sum_{\theta=0}^n \theta L_{\text{La:La,Ba:V}_a:\text{S}}^{\gamma-\text{La}_2\text{S}_3} (y'_{\text{La}} - y'_{\text{Ba}})^\theta + y'_{\text{La}} y''_{\text{La}} y''_{V_a} \sum_{\theta=0}^n \theta L_{\text{La:La:V}_a:\text{S}}^{\gamma-\text{La}_2\text{S}_3} (y''_{\text{La}} - y''_{V_a})^\theta + y'_{\text{Ba}} y''_{\text{La}} y''_{V_a} \sum_{\theta=0}^n \theta L_{\text{La:Ba:V}_a:\text{S}}^{\gamma-\text{La}_2\text{S}_3} (y''_{\text{La}} - y''_{V_a})^\theta, \quad (7c)$$

where y'_{La} and y'_{Ba} are the site fractions of La and Ba atoms in the first sublattice, y''_{La} and y''_{V_a} are the site fraction of La atoms and vacancies in the second sublattice. $G_{\text{La:La:V}_a:\text{S}}^{\gamma-\text{La}_2\text{S}_3}$, $G_{\text{La:La:La:S}}^{\gamma-\text{La}_2\text{S}_3}$ and $G_{\text{La:Ba:V}_a:\text{S}}^{\gamma-\text{La}_2\text{S}_3}$ are the Gibbs energy of the compounds La₂S₃, La₃S₄ (La_{2.25}S₃), BaLa₂S₄ (La_{1.5}Ba_{0.75}S₃). $G_{\text{La:Ba:La:S}}^{\gamma-\text{La}_2\text{S}_3}$ is the Gibbs energy of the hypothetical compound La_{1.25}Ba_{0.75}S₃.

3.3. Optimization methodology

We used the described models to calibrate thermodynamic descriptions for all the phases identified in the literature for the Ba–La–S and Ga–La–S systems (Tables 1 and 2). Specifically, we fitted the parameters in the Gibbs free energy functions to the experimental data reviewed in Section 2 as well as AIMD calculations carried out in this study for the liquid phases and described in Section 4.1. The parameters were optimized in the PanOptimizer module of the Pandat software [85].

4. Results and discussion

4.1. AIMD calculations of liquid phases

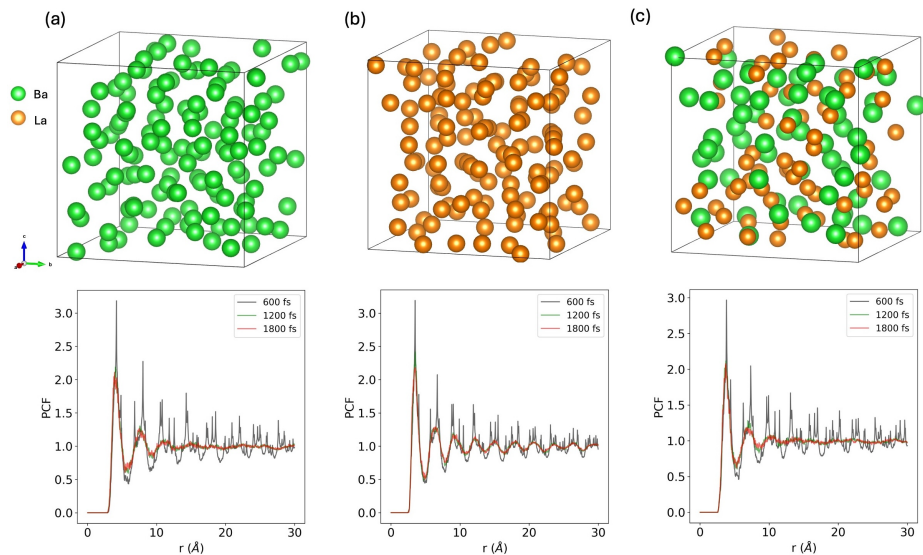


Figure 1: Representative equilibrium snapshots of the supercells for (a) pure Ba liquid, (b) pure La liquid, and (c) the 50 at.% Ba–La liquid alloy at 1600 K, as well as their corresponding PCFs at three time steps.

Snapshots of equilibrated structures and the corresponding PCFs (Figures 1 and 2) confirm the liquid state has been reached as targeted in the AIMD simulations. Peaks corresponding to the long-range order broaden with time and disappear by simulation time step of 1200 fs. The coincidence of the PCF curves at 1800 fs and 1200 fs further confirms the equilibrium condition reached within the time considered in the AIMD simulations.

Upon confirmation that equilibrium was reached in the liquid phases using AIMD, we calculated the mixing enthalpy of Ba–La, Ga–GaS, and La–LaS systems obtained with the simulations (symbols in Figure 3). All three systems show that mixing is energetically unfavorable compared to the pure components at the studied temperatures. The asymmetric composition dependence of the

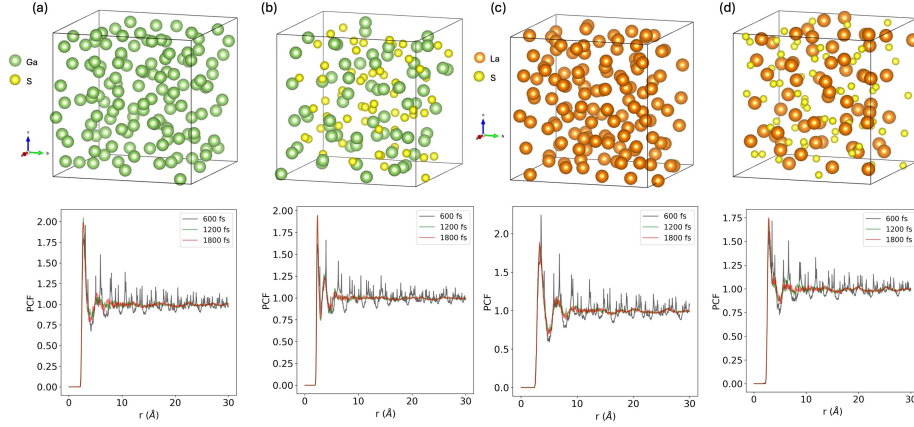


Figure 2: Representative equilibrium snapshots of the supercells for (a) pure Ga and (b) GaS liquids at 1600 K; (c) pure La and (d) LaS liquids at 3200 K as well as their corresponding PCFs at three time steps.

mixing enthalpy reflects the non-ideal interactions in the liquids. These mixing enthalpy values are adopted for fitting the interaction parameters of the relevant phases in our assessment and evaluating the assessment results (see Section 4.2). Additionally, the equilibrium supercell volumes at nearly zero internal pressure from AIMD simulations are presented (see inset in Figure 3).

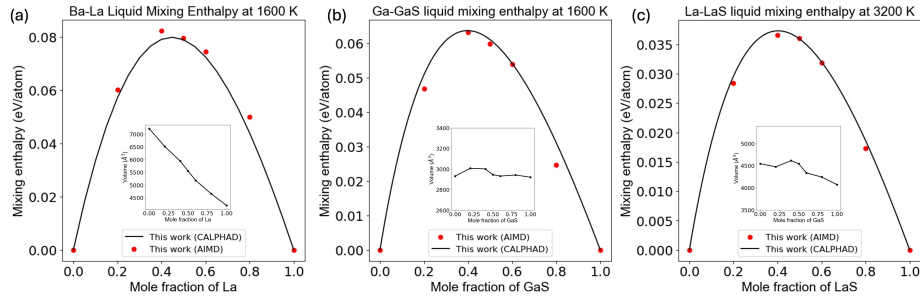


Figure 3: Mixing enthalpy of alloy liquids at various compositions for (a) Ba-La at 1600 K, (b) Ga-GaS at 1600 K, and (c) La-LaS at 3200 K. The mixing enthalpy from the present AIMD simulations (red symbols) and the ensuing CALPHAD assessment (black curves) are seen to be consistent. The inset shows the equilibrium supercell volumes at different compositions under nearly zero internal pressure.

4.2. Thermodynamic assessment

All phase diagrams obtained with the CALPHAD method in this study are presented in Figure 4 for the Ba-La-S system and Figure 7 for the Ga-La-S system along with the literature data available for these phase diagrams. Tables 3 and 6 lists the invariant reactions in the two systems – both calculated

in this study and reported in the literature. The sets of functions with calibrated parameters underlying these results are given in Tables 4, 5, 7 and 8. The thermodynamic properties calculated with these calibrated models are shown in Figures 5, 6 and 8. Overall, we observe good agreement between our calculations and data reported in the literature. Below, we discuss these results in more detail for both systems.

4.2.1. The Ba–La–S system

In the composition range where experimental data are available ($0.5 < x_S < 0.8$) [4, 13, 19, 20], the calculated Ba–S binary phase diagram (Figure 4(a)) reproduces the key features: the congruent melting point of BaS, the high-temperature phases ht-BaS₂ and BaS₃, and the phase transition between ht- and lt-BaS₂. Since multiple melting temperatures have been reported for BaS, we adopted the mean of the two consistent values from literature [19, 20], i.e., 2475 K. For rest of the Ba–S compounds, the assessment is calibrated to the only widely cited source [13]. To account for the experimentally observed steep liquidus line, strong associate interactions were introduced, enabling accurate reproduction of the available liquidus data and the corresponding solidus line.

The calculated Ba–La binary phase diagram (Figure 4(b)) reproduces the reported invariant reactions, including the limited solid solubilities in b.c.c.-Ba (0.2 at.%), b.c.c.-La (1.0 at.%), and f.c.c.-La, as well as the monotectic points at 0.4 and 90 at.%. The mixing enthalpy at 1600 K of the Ba–La liquid phase obtained in AIMD simulations (Figure 3(a)) was used as a supplement to the scarce experimental data. With the incorporation of AIMD constraints, the resulting CALPHAD description yields a phase diagram consistent with the only published experimental study [22].

For the La–S binary phase diagram (Figure 4(c)), experimental data are available up to 70 at.% sulfur content. Our assessment relied mainly on the comprehensive measurements of Kamarzin et al. [5], including the eutectic points between S and LaS and between LaS and γ -La₂S₃, the eutectic liquidus line of LaS– γ -La₂S₃, the liquidus of the γ -La₂S₃ solid solution, and the congruent melting of LaS. Since Kamarzin et al. did not report the melting of γ -La₂S₃, we adopted the values from Nikolaev and Vasileva [30]. The $\alpha \leftrightarrow \beta$ and $\beta \leftrightarrow \gamma$ phase transitions of La₂S₃ were taken from Picon et al. [27] and Eyring et al. [29], respectively. For LaS₂, the melting point reported by Le Rolland et al. [32] was used. Because the transition temperature between orthorhombic [32] and monoclinic [33] LaS₂ is ambiguous in the literature, these polymorphs were treated as a single phase in our assessment. In addition, La₃S₄ is unstable at room temperature according to our results, which is consistent with experimental observations [27, 28] and with DFT calculations from the Materials Project [86].

Both Ba–S and La–S phase diagrams include liquidus lines obtained according to the present assessment, which however currently lack experimental data. These liquidus lines may need further experimental validation (dashed lines in Figure 4(a,c)).

For the ternary Ba–La–S system, we focus on the BaS–La₂S₃ pseudo-binary phase diagram because it is the only section that has been experimentally in-

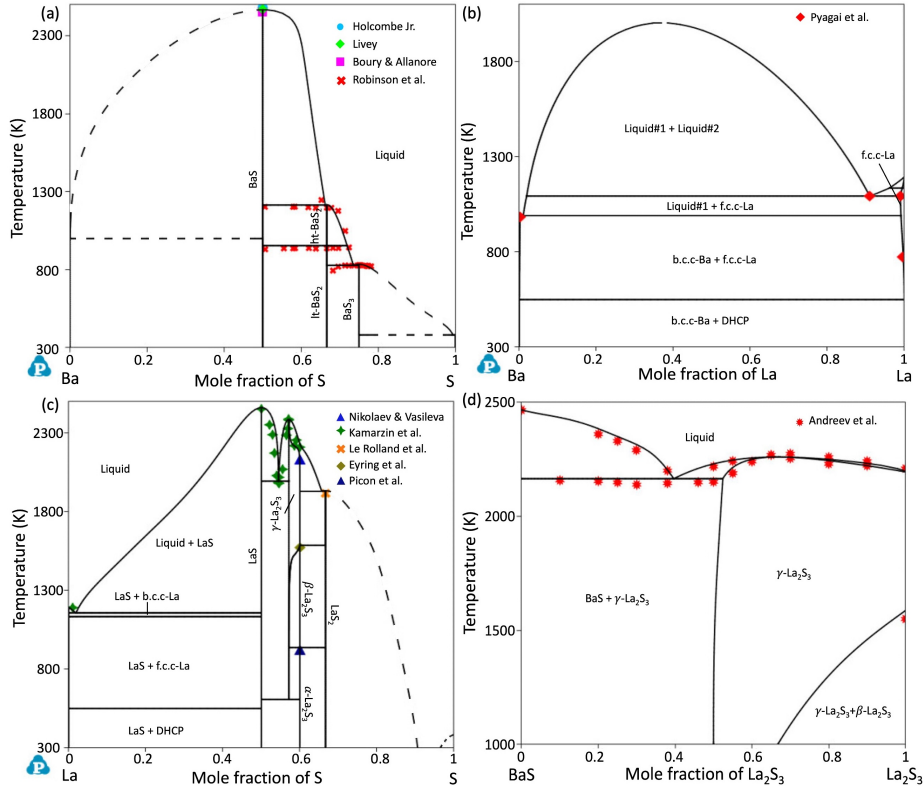


Figure 4: Phase diagrams calculated for the Ba-La-S system along with the literature data: (a) Ba-S; (b) Ba-La; (c) La-S; (d) BaS-La₂S₃. Symbols overlaid with the phase diagram lines represent literature data. The dashed lines represent calculated liquidus lines in regions currently lacking experimental data (and thus require further validation).

vestigated in the literature. For our assessment, we followed the comprehensive study by Andreev et al. [51], who reported an incongruent melting point for γ -La₂S₃ and large solubility of BaS in γ -La₂S₃. The melting points of both BaS and γ -La₂S₃ used in this work are consistent with other references [5, 6]. A pseudo-binary phase diagram calculated according to these data is shown in Figure 4(d).

We next present the thermodynamic properties of solid phases pertinent to the Ba-La-S system obtained as part of our assessment and their comparison with available experimental measurements and AIMD calculations.

Figure 5 presents the thermodynamic properties of the Ba-S system. The Gibbs formation energy and enthalpy increment of BaS over the temperature range 400 K to 1200 K obtained in our assessment show a good fit (Figure 5(a,b)) to the data from the NIST database [53], which served as the only source of experimental measurements of these properties for our model calibration. The heat capacity of BaS (Figure 5(c)) is compared to the experimental values from

the NIST database [53] and the first-principles calculations by Tuncel et al. [56] over the temperature range 350 K to 1000 K. Since DFT predictions neglected anharmonic contributions (as discussed in Section 2) and deviated from experiments at elevated temperatures, we only used the NIST data for parameter calibration and show DFT results for comparison.

Figure 5(d) shows the formation enthalpies at 298 K for Ba–S compounds, including BaS, low-temperature BaS₂, and BaS₃. For BaS, the NIST database reports $\Delta H(298K) = -231.8 \pm 2.1$ kJ/mol (shown as error bar in Figure 5(d)), which is consistent with our assessment giving the value of -232.2 kJ/mol. Additional reference data from the Materials Project [86], NBS [87], and recent DFT studies [88] are included for comparison.

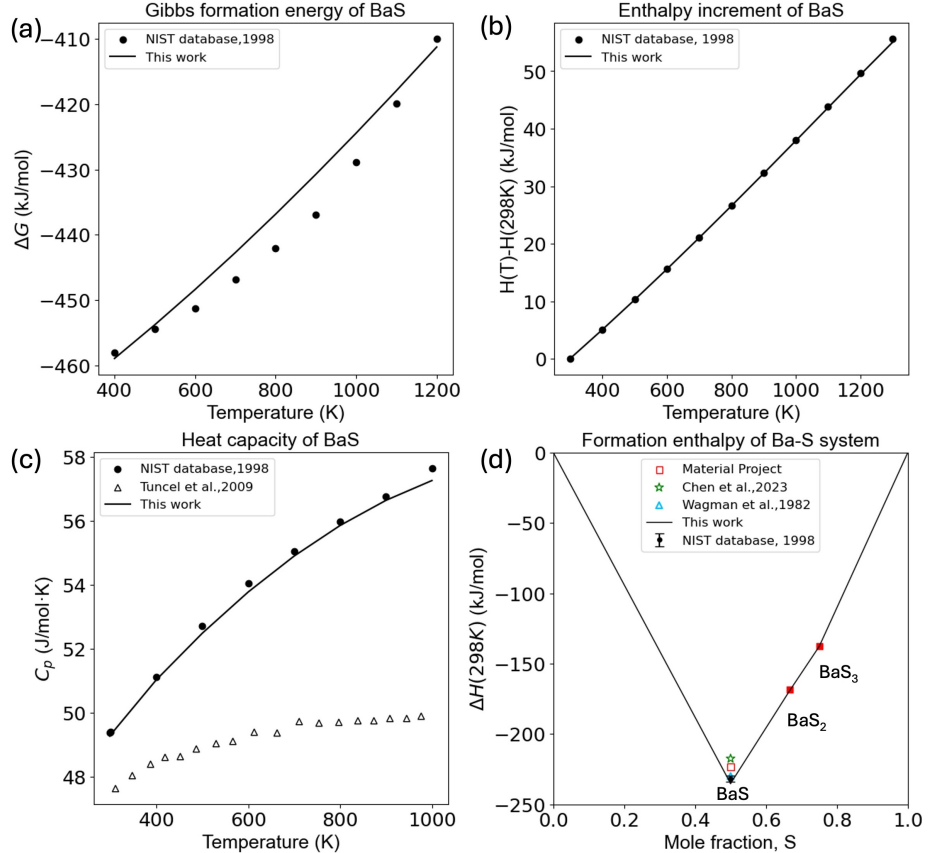


Figure 5: Thermodynamic properties for the Ba–S binary system: (a) formation Gibbs free energy, (b) enthalpy increment, and (c) heat capacity of BaS; (d) formation enthalpy of the Ba–S phases. Symbols represent literature data: filled for data included in the parameter calibration, open symbols for data shown only for comparison.

Thermodynamic properties of solid phases in the La–S binary system are summarized in Figure 6, including the heat capacity, enthalpy increment, en-

tropy and formation enthalpy from literature and our database. The properties of La–S compounds reported by Bolgar et al. [59] were mainly used for the assessment, and our database match well with the experimental data. Enthalpy increments were measured by Bolgar et al. [59] using high-temperature differential calorimeter with the measurement uncertainties of 0.75 % for LaS, 0.5 % for La₂S₃, 0.5 % for La₃S₄ and 1.1 % for LaS₂; these uncertainties were propagated to the derived heat capacity and entropy, $C_p(T)$ and $S(T)$.

Figure 6(a–c) shows the thermodynamic properties of LaS, including low-temperature heat capacity from Vasilev et al. [60] obtained with vacuum adiabatic calorimeter (Figure 6(a)). The two heat capacity sources [59, 60] cover different temperature ranges but overlap at room temperature, where their values agree. The enthalpy increment and entropy of LaS were fitted to the results of Bolgar et al. as the only available data source (Figure 6(b,c)).

Figure 6(d–f) show the properties of γ -La₂S₃. Several experimental studies report the heat capacity [59, 62–64] with good consistency around room temperature except the measurements by Vasilyeva and Nikolaev [64] at 900 K. The high-temperature discrepancy likely reflects methodological differences: Vasilyeva and Nikolaev [64] infer heat capacities indirectly from vapor-pressure equilibria that is sensitive to sulfur nonstoichiometry and volatility. Whereas Bolgar et al. [59] report direct high-temperature calorimetry on phase-verified La₂S₃ with stated uncertainties, which we adopt as the more reliable basis. Figure 6(e,f) show the enthalpy increment and entropy of γ -La₂S₃ which are consistent across studies for a wide range of temperatures. Our assessment therefore adopted representative data by Bolgar et al. [59] for parameter calibration, which results in a good agreement between the calculated and literature values (Figure 6(e,f)).

For La₃S₄, we adopted the thermodynamic property data from Bolgar et al. [59], which are in agreement with our results upon parameter calibration (Figure 6(g–i)). The enthalpy increment measurements of Amano et al. [62] align with those of Bolgar et al. at low temperatures but deviate significantly at higher temperatures. This discrepancy is likely due to impurities introduced by the preparation method employed by Amano et al., combined with their lack of detailed chemical composition data for the La₃S₄ samples. These reasons reinforce our choice for model calibration to the data from Bolgar et al. In addition, the DFT-calculated heat capacities of La₃S₄ by Viennois et al. [65] show good agreement with Bolgar et al. at room temperature and are included in Figure 6(g).

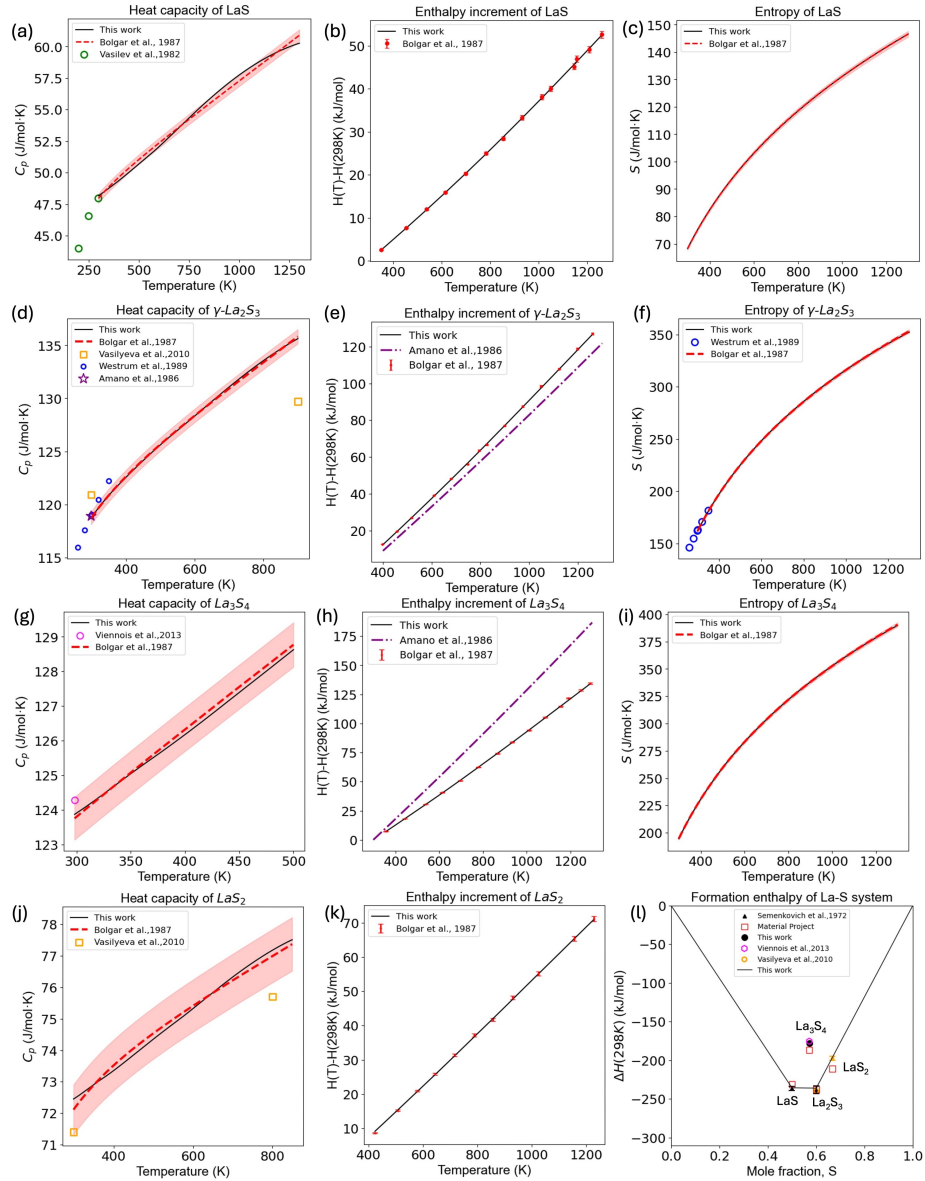


Figure 6: Thermodynamic properties for the La-S binary system: heat capacity, enthalpy increment, and entropy of (a–c) LaS; (d–f) γ -La₂S₃; (g–i) La₃S₄; (j–k) heat capacity and enthalpy increment of LaS₂ and formation enthalpy for the La-S phases. The shaded regions represent measurement uncertainty. Symbols represent literature data: filled for data included in the parameter calibration, open symbols for data shown only for comparison. Functional dependencies from literature are represented by lines: “dashed” for functions included in calibration, “dash-dotted” shown for reference only.

For less investigated LaS₂, the heat capacity of LaS₂ was reported by Vasi-

lyeva and Nikolaev [64] and by Bolgar et al. [59]. As shown in Figure 6(j), the two datasets are consistent at low temperatures but diverge at higher temperatures. Vasilyeva and Nikolaev report their value for 900 K by analogy to similar systems (PrS_2SmS_2) rather than from direct measurements. For this reason and because Bolgar et al. cover a broader temperature range, we adopted the data of Bolgar et al. in our assessment. Furthermore, as shown in Figure 6(k), our database calibrated the enthalpy increments to the data of Bolgar et al. and exhibits excellent agreement.

Figure 6(l) compares our calculated formation enthalpies of La–S phases at 298 K with literature data [61, 64, 65, 86]. The formation enthalpies of LaS and γ -La₂S₃ were calibrated to the experimental measurements of Semenkovich et al. [61] with measurement uncertainties of $\pm 2.5 \text{ kJ mol}^{-1}$ and $\pm 5 \text{ kJ mol}^{-1}$, respectively. For LaS₂, the value was calibrated to Vasilyeva et al. [64] with $\pm 2.6 \text{ kJ mol}^{-1}$ measurement uncertainty, as it represents the only available experimental dataset. In the case of La₃S₄, the formation enthalpy agrees with the DFT results of Viennois et al. [65] and lies above the convex hull, indicating its metastability at room temperature, which is consistent with the La–S phase diagram obtained in this study. For completeness, predictions from the Materials Project [86] are also included in the comparison.

4.2.2. The Ga–La–S system

The thermodynamic parameters obtained in the present work for the Ga–La–S system are listed in Tables 7 and 8. One binary phase diagram (Ga–S) and one pseudo-binary phase diagram (Ga₂S₃–La₂S₃) were calculated using the developed thermodynamic database and are shown in Figure 7.

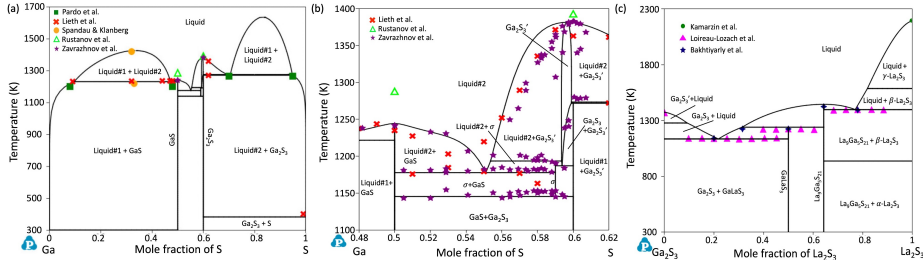


Figure 7: Phase diagrams calculated for the Ga–La–S system along with the literature data: (a) Ga–S and (b) its detailed view in the composition range (48 to 62 at.% sulfur) above 1100 K; (c) Ga₂S₃–La₂S₃. Symbols represent the literature data: filled for data used for the parameter calibration, open symbols for data shown only for comparison.

For the Ga–S binary phase diagram (Figure 7(a)), we adopted the experimental interpretation from widely cited studies [36–41], rather than the alternative version reported by Rustanov et al. [35]. Pardo et al. [36] and Lieth et al. [41] identified a miscibility gap on the Ga-rich side (from 10 to 48 at.% at 1203 K), while Pardo et al. additionally reported a second miscibility gap on the S-rich side (from 70 to 95 at.% at 1266 K). Furthermore, Spandau and Klanberg [39] measured the composition and temperature corresponding to the peak

of the Ga-rich miscibility gap. Our CALPHAD parameters were optimized to reproduce these invariant reaction points.

Figure 7(b) shows a section of the Ga–S binary phase diagram focusing on the composition range 48 to 62 at.% and the temperature interval 1100 K to 1400 K. Lieth et al. [41] and Zavrazhnov et al. [40] reported the consistent condition of invariant reactions and liquidus line. Zavrazhnov et al. [40] further identified three additional phases (σ , $\text{Ga}_2\text{S}_3'$, and $\gamma\text{-Ga}_2\text{S}_3$) within a narrow composition interval, together with three additional invariant reactions. Our database was optimized to these data and successfully reproduces the phase diagram.

The pseudo-binary $\text{Ga}_2\text{S}_3\text{-La}_2\text{S}_3$ phase diagram (Figure 7(c)) was assessed using phase transition data from Refs. [5, 10, 52], including the melting points of Ga_2S_3 , La_2S_3 , GaLaS_3 , and $\text{La}_9\text{Ga}_5\text{S}_{21}$, as well as the two eutectic reactions listed in Table 6. In the absence of experimental information on the liquidus line, our assessment targeted consistency with the reported invariant points [10].

Figure 8 summarizes the thermodynamic properties of phases in the Ga–S system. Our assessment adopted the heat capacity and entropy of Ga_2S_3 (Figure 8(a,b)) reported by Rika et al. [67], who combined experimental measurements with DFT calculations. The relaxation calorimetry data carry a measurement uncertainty of approximately 2 % in the temperature range from 40 to 300 K, while the Tian–Calvet calorimeter has a measurement uncertainty of about 1 % [67] (error bars in Figure 8(a)). For reference, the temperature dependence of the heat capacity estimated using the Neumann–Kopp rule by Moiseev and Sesták [66] is also included. Deviations in the two sources can be attributed to lattice vibrations, electronic contributions, and anharmonic or defect effects that are not captured by the purely additive assumption of the Neumann–Kopp rule. In addition, our assessment incorporated the heat capacity of GaS (Figure 8(c)) from Sedmidubský et al. [69], which is the only source of thermodynamic data for this phase. Their measurements, obtained using PPMS and DSC calorimetry, are reported with measurement uncertainties of approximately 2 % and 1 %, respectively [69]. Our assessment was primarily calibrated to the DSC results, owing to their broader temperature coverage and lower measurement uncertainty. For comparison, the data obtained from PPMS measurements and the Debye model are also plotted.

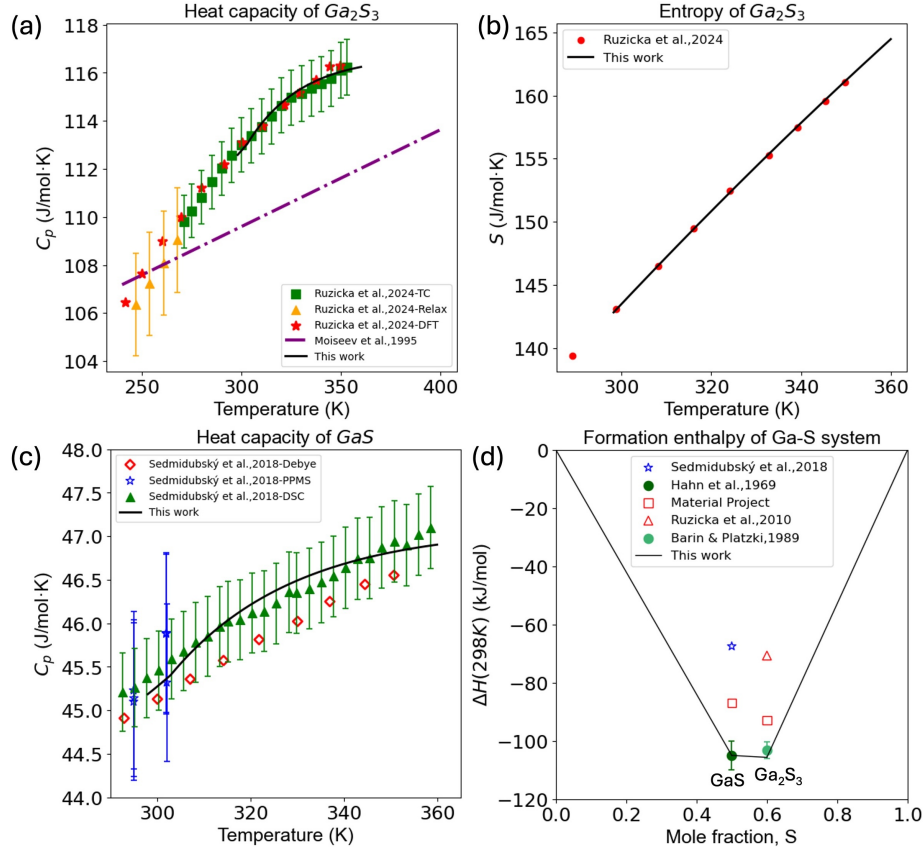


Figure 8: Thermodynamic properties for the Ga–S binary system: (a) heat capacity of Ga_2S_3 ; (b) entropy of Ga_2S_3 ; (c) heat capacity of GaS ; (d) formation enthalpy for the Ga–S system at 298 K. Symbols represent literature data: filled for data included in the parameter calibration, open symbols for data shown only for comparison; functional dependencies from literature are represented by lines: “dashed” for functions included in calibration, “dash-dotted” shown for reference only.

Figure 8(d) presents the formation enthalpies obtained in this study, calibrated to the widely cited experimental values of Hahn et al. [70] for GaS and Barin & Platzki [68] for Ga_2S_3 . The underestimation of GaS formation enthalpy by Sedmidubský et al. [69] (DFT) is likely related to the complex stacking sequence of the lamellar GaS microstructure, which has a non-trivial influence on the cohesive energy and thus on the calculated formation enthalpy [69]. For Ga_2S_3 , the discrepancy between the DFT value of Rika et al. [67] and thermochemical data Barin & Platzki [68] can be attributed to the neglect of finite-temperature contributions in the total energy used for the DFT-based estimation [67]. For comparison, Figure 8(d) also includes the DFT results of Sedmidubský et al. [69] for GaS , Rika et al. [67] for Ga_2S_3 , and the calculated values from the Materials Project [86] for both phases.

5. Conclusion

This paper reports the first thermodynamic assessment using the CALPHAD method for binary and pseudo-binary phase diagrams in the Ba–La–S and Ga–La–S systems. Following a thorough literature review, the study chose thermodynamic models appropriate to individual phases and calibrated the thermodynamic parameters to selected experimental and computational data. The assessment incorporated both phase diagram data and thermodynamic properties reported in literature, including the formation enthalpy, entropy, Gibbs energy of formation, and enthalpy increment. For liquid phases in the systems that lack reliable data, AIMD calculations were performed to estimate the mixing enthalpy and to complement the limited literature data. The resulting phase diagrams and calculated thermodynamic properties show good agreement with the available literature data and AIMD calculations in the explored compositional ranges of the binary and pseudo-binary phase diagrams. This study reports an assessment for systems with scarce data, limited to compositional ranges of $0.5 < x_S < 0.8$ in the Ba–S, $0.0 < x_S < 0.7$ in the La–S, and $0.0 < x_S < 0.6$ in the Ga–S systems. The calculated phase diagrams are accordingly most reliable only in these ranges. Outside of these ranges and for liquid phases at high temperatures, thermodynamic predictions should be considered provisional due to the lack of reliable experimental data. More detailed and refined CALPHAD models for these systems with strong application potential could greatly benefit from further experimental investigation of high-temperature phase equilibria and thermochemical properties in lanthanide chalcogenide (Ba–Ln–S, Ga–Ln–S) systems.

Data availability

The thermodynamic database (TDB) file is available in supplementary materials that allows reproducing the results of the present study.

Declaration of competing interest

The authors declare that they have no known competing financial interests or personal relationships that could have appeared to influence the work reported in this paper.

Acknowledgments

This work was supported by Air Force Office of Scientific Research grant No. FA9550-23-1-0167. We also thank Dr. Rushi Gong for fruitful discussions on the CALPHAD methodology.

| Reaction | T (K) | | Composition x_S | | |
|---|--|---------|---------------------------|---------|--|
| | Literature | Present | Literature | Present | |
| $L \leftrightarrow BaS$ (<i>Congruent</i>) | 2454 [4], 2470 [19], 2480 [20] (A. [4], DTA [19, 20]) | 2475 | 0.5 [4, 19, 20] | 0.5 | |
| $L+BaS \leftrightarrow ht\text{-}BaS_2$ (<i>Eutectic</i>) | 1198 [6] (TA) | 1206 | 0.667 [6] | 0.667 | |
| $ht\text{-}BaS_2 \leftrightarrow lt\text{-}BaS_2$ (<i>Phase transition</i>) | 973 [6] (TA) | 966 | 0.667 [6] | 0.667 | |
| $L+lt\text{-}BaS_2 \leftrightarrow BaS_3$ (<i>Eutectic</i>) | 827 [6] (TA) | 831 | 0.75 [6] | 0.75 | |
| $L \leftrightarrow b.c.c.\text{-}Ba + f.c.c.\text{-}La$ (<i>Monotectic</i>) | 983 [22] (DTA, XRD) | 983 | 0.004 [22] | 0.014 | |
| $L\#2 \leftrightarrow f.c.c.\text{-}La + L$ (<i>Monotectic</i>) | 1076 [22] (DTA, XRD) | 1083 | 0.9 [22] | 0.9 | |
| $L \leftrightarrow LaS+b.c.c.\text{-}La$ (<i>Eutectic</i>) | 1171 [6] (TA) | 1168 | 0.013 [6] | 0.014 | |
| $L \leftrightarrow LaS$ (<i>Congruent</i>) | 2453 [5] (TA) | 2473 | 0.5 [5] | 0.5 | |
| $L \leftrightarrow \gamma\text{-}La_2S_3$ (<i>Congruent</i>) | 2210 [5], 2133 [30] (TA [5], BP [30], A. [4]) | 2209 | 0.6 | 0.6 | |
| $\gamma\text{-}La_2S_3 \leftrightarrow \beta\text{-}La_2S_3$ (<i>Phase transition</i>) | 1573 [29] (DTA) | 1602 | 0.6 [29] | 0.6 | |
| $\beta\text{-}La_2S_3 \leftrightarrow \alpha\text{-}La_2S_3$ (<i>Phase transition</i>) | 923 [27] (DTA) | 931 | 0.6 [27] | 0.6 | |
| $L \leftrightarrow La_3S_4$ (<i>Congruent</i>) | 2383 [5] (TA) | 2395 | 0.571 [5] | 0.571 | |
| $L \leftrightarrow LaS+La_3S_4$ (<i>Eutectic</i>) | 1985 [5] (TA) | 2005 | 0.544 [5] | 0.54 | |
| $L \leftrightarrow LaS_2$ (<i>Congruent</i>) | 1917 [32] (TA) | 1921 | 0.667 [32] | 0.667 | |
| Reaction | T (K) | | Composition $x_{La_2S_3}$ | | |
| | Literature | Present | Literature | Present | |
| $L \leftrightarrow BaS+\gamma\text{-}La_2S_3$ (<i>Eutectic</i>) | 2150 [51] (DTA) | 2154 | 0.45 [51] | 0.41 | |

Table 3: Invariant reactions in the Ba-La-S system. Reaction types and experimental techniques from the literature sources are given in parentheses (A. is for thermal arrest, BP is for boiling point, TA is for unspecified thermal analysis).

| Phase | Calibrated functions and parameters |
|--|---|
| b.c.c.-Ba | ${}^oG_{\text{La}}^{\text{bcc-Ba}} = 10000$ ${}^oL_{\text{Ba},\text{La}}^{\text{bcc-Ba}} = 34000 - 59.82T$ |
| f.c.c.-La | ${}^oL_{\text{Ba}}^{\text{fcc-La}} = -5000$ ${}^oL_{\text{Ba},\text{La}}^{\text{fcc}} = 62000 - 99.71T$ |
| b.c.c.-La | ${}^oG_{\text{Ba}}^{\text{bcc-La}} = -1000 - 48T$ |
| BaS | ${}^oG_{\text{Ba:S}}^{\text{BaS}} = {}^oG_{\text{Ba}}^{\text{bcc-Ba}} + {}^oG_{\text{S}}^{\text{Orth}}$ $-470318.75 - 88.2T + 17.29T \ln(T) - 744851/T + 0.0016534T^2$ |
| ht-BaS ₂ | ${}^oG_{\text{Ba:S}}^{\text{ht-BaS}_2} = {}^oG_{\text{Ba}}^{\text{bcc-Ba}} + 2{}^oG_{\text{S}}^{\text{Orth}} - 505580 + 7.2T$ |
| lt-BaS ₂ | ${}^oG_{\text{Ba:S}}^{\text{lt-BaS}_2} = {}^oG_{\text{Ba}}^{\text{bcc-Ba}} + 2{}^oG_{\text{S}}^{\text{Orth}} - 507680 - 5T$ |
| BaS ₃ | ${}^oG_{\text{Ba:S}}^{\text{BaS}_3} = {}^oG_{\text{Ba}}^{\text{bcc}} + 3{}^oG_{\text{S}}^{\text{Orth}} - 551210 + 12T$ |
| LaS | ${}^oG_{\text{La:S}}^{\text{LaS}} = {}^oG_{\text{La}}^{\text{dhcp}} + {}^oG_{\text{S}}^{\text{Orth}}$ $-469002.32 - 9.33T + 4.29T \ln(T) - 117987.92/T$ |
| α -La ₂ S ₃ | ${}^oG_{\text{La:S}}^{\alpha\text{-La}_2\text{S}_3} = 2{}^oG_{\text{La}}^{\text{dhcp}} + 3{}^oG_{\text{S}}^{\text{Orth}} - 1226167 + 79T$ |
| β -La ₂ S ₃ | ${}^oG_{\text{La:S}}^{\beta\text{-La}_2\text{S}_3} = 2{}^oG_{\text{La}}^{\text{dhcp}} + 3{}^oG_{\text{S}}^{\text{Orth}}$ $-1224293 + 77T$ |
| LaS ₂ | ${}^oG_{\text{La:S}}^{\text{LaS}_2} = {}^oG_{\text{La}}^{\text{dhcp}} + 2{}^oG_{\text{S}}^{\text{Orth}}$ $-630548.97 + 11T + 0.0077T^2 - 202224.9/T$ |
| γ -La ₂ S ₃ | ${}^oG_{\text{La:La:Va:S}}^{\gamma\text{-La}_2\text{S}_3} = 2{}^oG_{\text{La}}^{\text{dhcp}} + 3{}^oG_{\text{S}}^{\text{Orth}}$ $-1177703.12 + 19.78T + 2.08T \ln(T) - 145168.13/T + 0.007935T^2$ ${}^oG_{\text{La:La:La:S}}^{\gamma\text{-La}_2\text{S}_3} = 2.25{}^oG_{\text{La}}^{\text{dhcp}} + 3{}^oG_{\text{S}}^{\text{Orth}}$ $-1241075.91 - 29.92T + 7.63T \ln(T) - 309022.23/T + 0.0076T^2$ ${}^oL_{\text{La:La:La:Va:S}}^{\gamma\text{-La}_2\text{S}_3} = -2000 + 2T$ ${}^oL_{\text{La:Ba:La:S}}^{\gamma\text{-La}_2\text{S}_3} = 0.75{}^oG_{\text{Ba}}^{\text{bcc}} + 1.5{}^oG_{\text{La}}^{\text{dhcp}} + 3{}^oG_{\text{S}}^{\text{Orth}} - 1377124 + 115T$ ${}^oL_{\text{La:Ba:Va:S}}^{\gamma\text{-La}_2\text{S}_3} = 0.75{}^oG_{\text{Ba}}^{\text{bcc}} + 1.25{}^oG_{\text{La}}^{\text{dhcp}} + 3{}^oG_{\text{S}}^{\text{Orth}}$ $-1299976 + 110.06T$ ${}^oL_{\text{La:Ba:La, Va:S}}^{\gamma\text{-La}_2\text{S}_3} = -10000$ ${}^oL_{\text{La:Ba, La:La:S}}^{\gamma\text{-La}_2\text{S}_3} = -12000$ ${}^oL_{\text{La:Ba, La:Va:S}}^{\gamma\text{-La}_2\text{S}_3} = -8000$ |

Table 4: Thermodynamic functions for the solid phases in the Ba–La–S system obtained in this work.

| Phase | Calibrated functions and parameters |
|---|---|
| Liquid (Ba,La,S,LaS,BaS,La ₂ S ₃) | ${}^oL_{\text{Ba,La}}^{\text{Liq}} = 30509.54$ ${}^1L_{\text{Ba,La}}^{\text{Liq}} = 6678.78$ ${}^oL_{\text{Ba,S}}^{\text{Liq}} = -300853$ ${}^oG_{\text{BaS}}^{\text{Liq}} = {}^oG_{\text{Ba}}^{\text{Liq}} + {}^oG_{\text{S}}^{\text{Liq}} - 279853 + 24T$ ${}^oL_{\text{BaS,S}}^{\text{Liq}} = -410000 - 40T$ ${}^oL_{\text{Ba,BaS}}^{\text{Liq}} = -110000$ ${}^oL_{\text{La,S}}^{\text{Liq}} = -344039$ ${}^oG_{\text{LaS}}^{\text{Liq}} = {}^oG_{\text{La}}^{\text{Liq}} + {}^oG_{\text{S}}^{\text{Liq}} - 442000 + 44T$ ${}^oG_{\text{La}_2\text{S}_3}^{\text{Liq}} = 2{}^oG_{\text{La}}^{\text{Liq}} + 3{}^oG_{\text{S}}^{\text{Liq}} - 867000 + 112T$ ${}^oL_{\text{LaS,La}_2\text{S}_3}^{\text{Liq}} = -639000$ ${}^oL_{\text{La,La}_2\text{S}_3}^{\text{Liq}} = -440000 - 25T$ ${}^oL_{\text{La,LaS}}^{\text{Liq}} = 20800 - 25T$ ${}^1L_{\text{La,LaS}}^{\text{Liq}} = 1000$ ${}^oL_{\text{La}_2\text{S}_3,\text{S}}^{\text{Liq}} = -240000 - 49T$ ${}^oL_{\text{LaS,S}}^{\text{Liq}} = -240000 - 20T$ ${}^oL_{\text{Ba,La,S}}^{\text{Liq}} = -457411$ ${}^oL_{\text{BaS,LaS}}^{\text{Liq}} = -187391$ ${}^1L_{\text{BaS,LaS}}^{\text{Liq}} = 40000$ ${}^2L_{\text{BaS,LaS}}^{\text{Liq}} = 101739$ ${}^oL_{\text{BaS,La}_2\text{S}_3}^{\text{Liq}} = -498386$ ${}^1L_{\text{BaS,La}_2\text{S}_3}^{\text{Liq}} = 50000$ ${}^2L_{\text{BaS,La}_2\text{S}_3}^{\text{Liq}} = 128385$ |

Table 5: Thermodynamic functions for the liquid phases in the Ba–La–S system obtained in this work.

| Reaction | T (K) | | Composition x_S | |
|---|---------------------------------|---------|---------------------------|---------|
| | Literature | Present | Literature | Present |
| $L \leftrightarrow GaS$ (<i>Congruent</i>) | 1288 [6], 1235 [41] (TA, TA) | 1293 | 0.5 [6, 41] | 0.5 |
| $L \leftrightarrow Ga_2S_3$ (<i>Congruent</i>) | 1393 [6], 1363 [41] (TA, TA) | 1390 | 0.6 [6, 41] | 0.6 |
| $L \leftrightarrow GaS + \sigma$ (<i>Eutectic</i>) | 1182 [40] (DTA) | 1177 | 0.55 [40] | 0.55 |
| $\sigma \leftrightarrow Ga_2S_3' + L$ (<i>Peritectic</i>) | 1195 [40] (DTA) | 1195 | 0.59 [40] | 0.59 |
| $\sigma + Ga_2S_3 \leftrightarrow Ga_2S_3'$ (<i>Peritectic</i>) | 1184 [40] (DTA) | 1193 | 0.595 [40] | 0.593 |
| $Ga_2S_3 \leftrightarrow Ga_2S_3' + L$ (<i>Peritectic</i>) | 1279 [40] (DTA) | 1277 | 0.6 [40] | 0.6 |
| $L\#2 \leftrightarrow GaS + L$ (<i>Monotectic</i>) | 1237 [41] (TA) | 1232 | 0.47 [41] | 0.47 |
| $L\#2 \leftrightarrow Ga_2S_3 + L$ (<i>Monotectic</i>) | 1266 [36] (TA) | 1272 | 0.7 [36] | 0.7 |
| Reaction | T (K) | | Composition $x_{La_2S_3}$ | |
| | Literature | Present | Literature | Present |
| $L \leftrightarrow Ga_2S_3 + LaGaS_3$ (<i>Eutectic</i>) | 1057 [89] (DSC) | 1041 | 0.2 [10] | 0.21 |
| $L + La_9Ga_5S_{21} \leftrightarrow LaGaS_3$ (<i>Peritectic</i>) | 1225 [10] (TA) | 1215 | 0.5 [10] | 0.5 |
| $L \leftrightarrow La_9Ga_5S_{21}$ (<i>Congruent</i>) | 1425 [10] (TA) | 1417 | 0.643 [10] | 0.643 |
| $L \leftrightarrow La_9Ga_5S_{21} + \beta-La_2S_3$ (<i>Eutectic</i>) | 1395 [10] (TA) | 1376 | 0.8 [10] | 0.78 |

Table 6: Invariant reactions in the Ga-La-S system. Reaction types and experimental methods from literature sources are given in parentheses (TA is for unspecified thermal analysis, DTA is for differential thermal analysis, DSC is for differential scanning calorimetry).

| Phase | Calibrated functions and parameters |
|---------------------------------------|---|
| GaS | ${}^oG_{\text{Ga:S}}^{\text{GaS}} = {}^oG_{\text{Ga}}^{\text{Orth}} + {}^oG_{\text{S}}^{\text{Orth}}$ $-207924.33 - 14.53T + 4.13T \ln(T) - 91433.25/T + 0.0026T^2$ |
| Ga_2S_3 | ${}^oG_{\text{Ga:S}}^{\text{Ga}_2\text{S}_3} = 2 {}^oG_{\text{Ga}}^{\text{Orth}} + 3 {}^oG_{\text{S}}^{\text{Orth}}$ $-512346.89 - 11.98T + 4.62T \ln(T) - 209796.95/T + 0.0131T^2$ |
| $\text{Ga}_2\text{S}_3'$ | ${}^oG_{\text{Ga:Ga;S}}^{\text{Ga}_2\text{S}_3'} = 0.41 {}^oG_{\text{Ga}}^{\text{Orth}} + 0.59 {}^oG_{\text{S}}^{\text{Orth}} - 92969 - 0.6T$ ${}^oG_{\text{Ga:Va;S}}^{\text{Ga}_2\text{S}_3'} = 0.39 {}^oG_{\text{Ga}}^{\text{Orth}} + 0.59 {}^oG_{\text{S}}^{\text{Orth}} - 91869 + 1.1T$ ${}^oG_{\text{Ga:Ga,Va;S}}^{\text{Ga}_2\text{S}_3'} = -14800 + 10.3T$ |
| σ | ${}^oG_{\text{Ga:S}}^{\sigma} = 0.41 {}^oG_{\text{Ga}}^{\text{Orth}} + 0.59 {}^oG_{\text{S}}^{\text{Orth}} - 102634 + 7.26T$ |
| GaLaS_3 | ${}^oG_{\text{Ga:La;S}}^{\text{GaLaS}_3} = {}^oG_{\text{Ga}}^{\text{Orth}} + {}^oG_{\text{La}}^{\text{dhcp}} + 3 {}^oG_{\text{S}}^{\text{Orth}}$ $-1107000 + 105T$ |
| $\text{Ga}_5\text{La}_9\text{S}_{21}$ | ${}^oG_{\text{Ga:La;S}}^{\text{Ga}_5\text{La}_9\text{S}_{21}} = 5 {}^oG_{\text{Ga}}^{\text{Orth}} + 9 {}^oG_{\text{La}}^{\text{dhcp}} + 21 {}^oG_{\text{S}}^{\text{Orth}}$ $-7996381 + 890T$ |

Table 7: Thermodynamic functions for the solid phases in the Ga–La–S system obtained in this work. The La–S binary parameters are listed in Table 4. The Ga–La binary parameters are adopted from Ref. [12].

| Phase | Calibrated functions and parameters |
|---|--|
| Liquid | ${}^oL_{\text{Ga},\text{S}}^{\text{Liq}} = -74639$ |
| (Ga,La,S,GaS,Ga ₂ S ₃ ,LaS,La ₂ S ₃) | ${}^oG_{\text{Ga}_2\text{S}_3}^{\text{Liq}} = {}^oG_{\text{Ga}}^{\text{Liq}} + {}^oG_{\text{S}}^{\text{Liq}} - 157881$ ${}^oG_{\text{Ga}_2\text{S}_3}^{\text{Liq}} = 2 {}^oG_{\text{Ga}}^{\text{Liq}} + 3 {}^oG_{\text{S}}^{\text{Liq}} - 371000 + 30T$ ${}^oG_{\text{GaS},\text{Ga}_2\text{S}_3}^{\text{Liq}} = -116000$ ${}^1G_{\text{GaS},\text{Ga}_2\text{S}_3}^{\text{Liq}} = 60000$ ${}^oG_{\text{Ga},\text{GaS}}^{\text{Liq}} = 35363 - 8.5T$ ${}^1G_{\text{Ga},\text{GaS}}^{\text{Liq}} = 2500$ ${}^oG_{\text{Ga}_2\text{S}_3,\text{S}}^{\text{Liq}} = -45000$ ${}^1G_{\text{Ga}_2\text{S}_3,\text{S}}^{\text{Liq}} = -17000$ ${}^2G_{\text{Ga}_2\text{S}_3,\text{S}}^{\text{Liq}} = 13000$ ${}^oG_{\text{GaS},\text{S}}^{\text{Liq}} = -33000$ ${}^1G_{\text{GaS},\text{S}}^{\text{Liq}} = -38000$ ${}^oG_{\text{GaS},\text{La}_2\text{S}_3}^{\text{Liq}} = -590000$ ${}^2G_{\text{GaS},\text{La}_2\text{S}_3}^{\text{Liq}} = -100000$ ${}^oG_{\text{Ga}_2\text{S}_3,\text{LaS}}^{\text{Liq}} = -410000$ ${}^1G_{\text{Ga}_2\text{S}_3,\text{LaS}}^{\text{Liq}} = 100000$ ${}^oG_{\text{GaS},\text{LaS}}^{\text{Liq}} = -390000$ ${}^1G_{\text{GaS},\text{LaS}}^{\text{Liq}} = 100000$ ${}^2G_{\text{GaS},\text{LaS}}^{\text{Liq}} = -260000$ ${}^oG_{\text{Ga}_2\text{S}_3,\text{La}_2\text{S}_3}^{\text{Liq}} = -780000 - 80T$ ${}^1G_{\text{Ga}_2\text{S}_3,\text{La}_2\text{S}_3}^{\text{Liq}} = -20000$ |

Table 8: Thermodynamic functions for the liquid phases in the Ga–La–S system obtained in this work. The La–S binary parameters are listed in Table 5. The Ga–La binary parameters are adopted from Ref. [12].

References

- [1] W. B. White, Refractory sulfides as ir window materials, in: Window and Dome Technologies and Materials II, Vol. 1326, SPIE, 1990, pp. 80–92.
- [2] J. S. McCloy, B. J. Riley, D. A. Pierce, B. R. Johnson, A. Qiao, Infrared-transmitting glass–ceramics: a review, in: Proc. SPIE, Vol. 8708, 2013, p. 87080N.
- [3] J. S. McCloy, B. J. Riley, D. A. Pierce, Infrared-transparent glass ceramics: An exploratory study, Journal of Non-Crystalline Solids 410 (2015) 160–173.
- [4] C. Boury, A. Allanore, Liquid state properties and solidification features of the pseudo binary bas-la₂s₃, Scientific Reports 11 (1) (2021) 18189.

- [5] A. Kamarzin, K. Mironov, V. Sokolov, Y. N. Malovitsky, I. Vasil'Yeva, Growth and properties of lantanum and rare-earth metal sesquisulfide crystals, *Journal of Crystal Growth* 52 (1981) 619–622.
- [6] T. Massalski, H. Okamoto, P. Subramanian, L. Kacprzak, Binary alloy phase diagrams asm international, Okamoto, PR Subramanian, L. Kacprzak.–1996.–852 p (1990).
- [7] P. Kumta, S. Risbud, Rare-earth chalcogenides an emerging class of optical materials, *Journal of materials science* 29 (1994) 1135–1158.
- [8] B. Hallstedt, The sgte collection of binary datasets, *Calphad* 89 (2025) 102833.
- [9] E. Petracovschi, M. Hubert, J.-L. Adam, X.-H. Zhang, L. Calvez, Synthesis of ge s e4 glass by mechanical alloying and sintering, *physica status solidi (b)* 251 (7) (2014) 1330–1333.
- [10] A.-M. Loireau-Lozac'h, M. Guittard, J. Flahaut, Systèmes l2s3-ga2s3 (l= la, ce, dy, er et y) diagrammes de phases, *Materials Research Bulletin* 12 (9) (1977) 881–886.
- [11] H. Lukas, S. G. Fries, B. Sundman, Computational thermodynamics: the Calphad method, Cambridge university press, 2007.
- [12] S. Boudraa, Y. Djaballah, Y. Mansouri, A. B. Bouzida, Thermodynamic assessment of the ga–la and ga–pr systems supported by ab-initio calculations, *Calphad* 76 (2022) 102387.
- [13] P. L. Robinson, W. E. Scott, Xcv.the polysulphides of barium and calcium, *Journal of the Chemical Society (Resumed)* (1931) 693–709.
- [14] E. Jak, P. Hayes, Phase equilibria determination in complex slag systems, *Mineral Processing and Extractive Metallurgy* 117 (1) (2008) 1–17.
- [15] Y. Feutelais, B. Legendre, R. De Avillez, Standard enthalpy of formation of the ζ -phase in the fe–zn system at 298 k, *Journal of alloys and compounds* 346 (1-2) (2002) 211–216.
- [16] I. Kawada, K. Kato, S. Yamaoka, Barium disulphide, *Acta Crystallographica Section B: Structural Crystallography and Crystal Chemistry* 31 (12) (1975) 2905–2906.
- [17] S. Holgersson, Die struktur der sulfide von mg, ca, sr und ba, *Zeitschrift für anorganische und allgemeine Chemie* 126 (1) (1923) 179–182.
- [18] O. Güntert, A. Faessler, Präzisionsbestimmung der gitterkonstanten der erdalkalisulfide mgs, cas, srs und bas, *Zeitschrift für Kristallographie* 107 (5-6) (1956) 357–361.

- [19] D. Livey, The high temperature stability of oxides and sulphides, *J. less-common Metals* 1 (1959).
- [20] C. Holcombe Jr, Tentative cef3-bas phase diagram, *Journal of the Less Common Metals* 102 (1) (1984) L1–L3.
- [21] S. Yamaoka, J. Lemley, J. Jenks, H. Steinfink, Structural chemistry of the polysulfides dibarium trisulfide and monobarium trisulfide, *Inorganic Chemistry* 14 (1) (1975) 129–131.
- [22] I. Pegaj, A. Vakhobov, Phase diagrams of systems barium-lanthanum and aluminium-barium-lanthanum, in: *Dokl. Akad. Nauk Tadzh. SSR*, Vol. 28, 1985, pp. 718–721.
- [23] K. Mironov, I. Vasil'eva, A. Kamarzin, V. Sokolov, Y. N. Malovitskii, Phase diagram of the la-s system, *Izv. Akad. Nauk SSSR, Neorg. Mater.;(USSR)* 14 (4) (1978).
- [24] K. Westerholt, H. Endrikat, R. Dahlbeck, H. Bach, J. Sanchez, J. Friedt, Magnetic phase diagram of eu x la 1- x s, *Physical Review B* 33 (1) (1986) 567.
- [25] A. R. West, Basic solid state chemistry, (No Title) (1999).
- [26] C. T. Prewitt, A. W. Sleight, Structure of gadolinium sesquisulfide, *Inorganic Chemistry* 7 (6) (1968) 1090–1093.
- [27] M. Picon, M. Patrie, Sur les sous-sulfures des terres rares cériques, *Comptes rendus hebdomadaires des séances de l'Académie des Sciences* (1956) 1321–1324.
- [28] T. Schleid, F. Lissner, M10s140-type oxysulphides (m=la, ce, pr, nd, sm) as an oxygen trap in oxidation reactions of reduced lanthanide chlorides with sulphur, *Journal of the Less common Metals* 175 (2) (1991) 309–319.
- [29] L. Eyring, K. A. Gschneidner, G. Lander, *Handbook on the physics and chemistry of rare earths*, Vol. 32, Elsevier, 2002.
- [30] P. Nikolaev, I. Vasileva, Vapor pressure determination for solid and liquid la 2 s 3 using boiling points, *Inorganic Materials* 44 (2008) 1367–1371.
- [31] I. Vasilyeva, R. Nikolaev, High-temperature solid–vapor and liquid–vapor transitions in binary and ternary chalcogenides la2s3, mos2, mo2s3 and liinse2, *Journal of alloys and compounds* 452 (1) (2008) 89–93.
- [32] B. Rolland Le, P. McMillan, P. Colombet, Vibrational study of las2, ces2, prs2 and nds2 (1991).
- [33] J. Dugué, D. Carré, M. Guittard, Structure cristalline du polysulfure de lanthane las2, *Structural Science* 34 (2) (1978) 403–406.

- [34] A. Y. Zavrazhnov, D. Turchen, E. G. Goncharov, V. Zlomanov, Manometric method for the study of ptx diagrams, *Journal of phase equilibria* 22 (4) (2001) 482–490.
- [35] P. Rustanov, B. Mardakhaev, M. Safarov, The investigation of the ga-s system, *Inorg Mater* 3 (3) (1967) 429–33.
- [36] M. Pardo, M. Guittard, A. Chilouet, A. Tomas, Diagramme de phases gallium-soufre et études structurales des phases solides, *Journal of Solid State Chemistry* 102 (2) (1993) 423–433.
- [37] V. Zlomanov, A. Novoselova, Ptx phase diagrams of metal-chalcogen systems (1987).
- [38] J. Greenberg, Thermodynamic basis of crystal growth: PTX phase equilibrium and non-stoichiometry, Vol. 44, Springer Science & Business Media, 2001.
- [39] H. Spandau, F. Klanberg, Thermische untersuchungen an sulfiden. ii. das thermische verhalten der sulfide des galliums, *Zeitschrift für anorganische und allgemeine Chemie* 295 (5-6) (1958) 300–308.
- [40] A. Zavrazhnov, S. Berezin, A. Kosykov, A. Naumov, M. Berezina, N. Brezhnev, The phase diagram of the ga-s system in the concentration range of 48.0–60.7 mol% s, *Journal of Thermal Analysis and Calorimetry* 134 (1) (2018) 483–492.
- [41] R. Lieth, H. Heijligers, C. vd Heijden, The p-t-x phase diagram of the system ga-s, *Journal of the Electrochemical Society* 113 (8) (1966) 798.
- [42] P. Newman, J. Brice, H. Wright, The phase diagram of the gallium-tellurium system, *Philips Res. Repts.* 16 (1961) 41–50.
- [43] E. G. Grochowski, D. R. Mason, G. A. Schmitt, P. H. Smith, The phase diagram for the binary system indium-tellurium and electrical properties of in₃te₅, *Journal of Physics and Chemistry of Solids* 25 (6) (1964) 551–558.
- [44] M. Hansen, Constitution of binary alloys (1958).
- [45] S. S. Berezin, A. Y. Zavrazhnov, A. V. Naumov, I. N. Nekrylov, N. Y. Brezhnev, ga-s 48.0–60.7 % s, *Kondensirovannye sredy i mezhfaznye granitsy= Condensed Matter and Interphases* 19 (3) (2017) 321–335.
- [46] Y. Shimomura, K. Hayashi, H. Akamatsu, First-principles prediction of ferroelectricity in defective wurtzite α -ga₂s₃, *Japanese Journal of Applied Physics* 63 (8) (2024) 08SP12.
- [47] B. Krebs, A. Schiemann, M. Läge, Synthese und kristallstruktur einer neuen hexagonalen modifikation von al₂s₃ mit fünffach koordiniertem aluminium, *Zeitschrift für anorganische und allgemeine Chemie* 619 (6) (1993) 983–988.

[48] H. Hahn, W. Klingler, Ueber die kristallstrukturen von ga_2s_3 , ga_2se_3 und ga_2te_3 , Zeitschrift für anorganische Chemie 259 (1-4) (1949) 135–142.

[49] J. t. Goodyear, G. Steigmann, The crystal structure of α - ga_2s_3 , Acta Crystallographica 16 (10) (1963) 946–949.

[50] C. Jones, J. Bryan, K. Kirschbaum, J. Edwards, Refinement of the crystal structure of digallium trisulfide, ga_2s_3 , Zeitschrift für Kristallographie-New Crystal Structures 216 (1-4) (2001) 349–350.

[51] O. Andreev, A. Kertman, V. Bamburov, Interaction in systems bas- ln 2 s 3 ($ln = la, nd$), Zhurnal Neorganicheskoy Khimii 36 (10) (1991) 2623–2627.

[52] I. Bakhtiyarly, A. Abdullayeva, R. Kurbanova, R. Karimov, The ternary system la_2 , Azerbaijan Chemical Journal (3) (2016) 113–120.

[53] M. W. Chase, Nist-janaf thermochemical tables 4th ed., J. of Physical and Chemical Reference Data (1998) 1529–1564.

[54] E. G. King, W. Weller, Low-temperature heat capacities and entropies at 298.15 K. of the zirconates of calcium, strontium, and barium, Vol. 5571, US Department of the Interior, Bureau of Mines, 1960.

[55] O. Kubaschewski, Metallurgical thermochemistry, International Series on Material Science and Technology 24 (1977) 478.

[56] E. Tuncel, K. Colakoglu, E. Deligoz, Y. Ciftci, A first-principles study on the structural, elastic, vibrational, and thermodynamical properties of ba_x ($x = s, se$, and te), Journal of Physics and Chemistry of Solids 70 (2) (2009) 371–378.

[57] J. P. Rino, An interaction potential for barium sulfide: A molecular dynamics study, Computational materials science 92 (2014) 334–342.

[58] S. Baroni, S. De Gironcoli, A. Dal Corso, P. Giannozzi, Phonons and related crystal properties from density-functional perturbation theory, Reviews of modern Physics 73 (2) (2001) 515.

[59] A. Bolgar, A. Kriklya, L. Kartuzova, Enthalpy and heat capacity of lanthanum sulfides, Sov. Powder Metall. Met. Ceram.(Engl. Transl.);(United States) 26 (2) (1987).

[60] L. Vasilev, V. Grabov, A. Golubkov, A. Gorobets, V. Oskotskii, I. Smirnov, V. Tikhonov, Physical properties and phase transitions of the rare earth monosulphides in the homogeneity range, physica status solidi (a) 80 (1) (1983) 237–244.

[61] S. Semenkovich, V. Sergeeva, A. Finogenov, Enthalpies of formation of some rare-earth sulfides, Chemical Bonds in Solids: Volume 3: X-Ray and Thermodynamic Investigations (1972) 163–170.

- [62] T. Amano, B. Beaudry, K. Gschneidner Jr, High-temperature thermodynamic properties of alpha and gamma lanthanum sesquisulfides and related compounds, *Journal of applied physics* 59 (10) (1986) 3437–3440.
- [63] E. F. Westrum Jr, R. Burriel, J. B. Gruber, P. E. Palmer, B. J. Beaudry, W. Plautz, Thermophysical properties of the lanthanide sesquisulfides. i. schottky functions and magnetic and electronic properties of γ -la₂s₃, γ -ce₂s₃, γ -nd₂s₃, and γ -gd₂s₃, *The Journal of chemical physics* 91 (8) (1989) 4838–4848.
- [64] I. G. Vasilyeva, R. Nikolaev, The la₂s₃–las₂ system: Thermodynamic and kinetic study, *Journal of Solid State Chemistry* 183 (8) (2010) 1747–1751.
- [65] R. Viennois, K. Niedziolka, P. Jund, Physical properties of the thermoelectric cubic lanthanum chalcogenides la₃- y x 4 (x= s, se, te) from first principles, *Physical Review B Condensed Matter and Materials Physics* 88 (17) (2013) 174302.
- [66] G. Moiseev, J. Šesták, Thermochemical and thermodynamical properties of some compounds in the system ga- sb- s, *Journal of Thermal Analysis and Calorimetry* 43 (2) (1995) 539–544.
- [67] K. Růžička, V. Pokorný, J. Plutnar, I. Plutnarová, B. Wu, Z. Sofer, D. Sedmidubský, Heat capacity of indium or gallium sesqui-chalcogenides, *Materials* 17 (2) (2024) 361.
- [68] I. Barin, G. Platzki, *Thermochemical data of pure substances*, Vol. 304, VCh Weinheim, 1989.
- [69] D. Sedmidubský, Z. Sofer, Š. Huber, J. Luxa, R. Točík, T. Mahnel, K. Růžička, Chemical bonding and thermodynamic properties of gallium and indium monochalcogenides, *The Journal of Chemical Thermodynamics* 128 (2019) 97–102.
- [70] H. Hahn, F. Burow, Über die bildungsenthalpien der sulfide, selenide und telluride des galliums und indiums, in: *Angewandte Chemie-International Edition*, Vol. 68, WILEY-V CH VERLAG GMBH MUHLENSTRASSE 33-34, D-13187 BERLIN, GERMANY, 1956, pp. 382–382.
- [71] G. Kresse, J. Hafner, Ab initio molecular dynamics for liquid metals, *Physical review B* 47 (1) (1993) 558.
- [72] G. Kresse, J. Furthmüller, Efficiency of ab-initio total energy calculations for metals and semiconductors using a plane-wave basis set, *Computational materials science* 6 (1) (1996) 15–50.
- [73] J. P. Perdew, J. A. Chevary, S. H. Vosko, K. A. Jackson, M. R. Pederson, D. J. Singh, C. Fiolhais, Atoms, molecules, solids, and surfaces: Applications of the generalized gradient approximation for exchange and correlation, *Physical review B* 46 (11) (1992) 6671.

[74] G. Kresse, D. Joubert, From ultrasoft pseudopotentials to the projector augmented-wave method, *Physical review b* 59 (3) (1999) 1758.

[75] W. G. Hoover, Canonical dynamics: Equilibrium phase-space distributions, *Physical review A* 31 (3) (1985) 1695.

[76] S. Nosé, A unified formulation of the constant temperature molecular dynamics methods, *The Journal of chemical physics* 81 (1) (1984) 511–519.

[77] N. N. Greenwood, A. Earnshaw, *Chemistry of the Elements*, Elsevier, 2012.

[78] A. T. Dinsdale, Sgte data for pure elements, *Calphad* 15 (4) (1991) 317–425.

[79] O. Redlich, A. Kister, Thermodynamics of nonelectrolyte solutions-xyt relations in a binary system, *Industrial & Engineering Chemistry* 40 (2) (1948) 341–345.

[80] H. Kopp, Iii. investigations of the specific heat of solid bodies, *Philosophical Transactions of the Royal Society of London* (155) (1865) 71–202.

[81] R. Gong, S.-L. Shang, Y. Wang, J. P. S. Palma, H. Kim, Z.-K. Liu, Revisiting thermodynamics in (lif, naf, kf, crf2)–crf3 by first-principles calculations and calphad modeling, *Calphad* 85 (2024) 102703.

[82] B.-C. Zhou, S.-L. Shang, Z.-K. Liu, First-principles calculations and thermodynamic modeling of the sn- sr and mg- sn- sr systems, *Calphad* 46 (2014) 237–248.

[83] R. Schmid, Y. A. Chang, A thermodynamic study on an associated solution model for liquid alloys, *Calphad* 9 (4) (1985) 363–382.

[84] X. Zhang, G. Wenhua, W. Qian, Z. Qingfeng, Structural, phonon, mechanical, optical, and thermodynamic properties of stable β -la2s3 from first-principles calculations, *Journal of Rare Earths* 35 (3) (2017) 271–279.

[85] S.-L. Chen, S. Daniel, F. Zhang, Y. Chang, X.-Y. Yan, F.-Y. Xie, R. Schmid-Fetzer, W. Oates, The pandat software package and its applications, *Calphad* 26 (2) (2002) 175–188.

[86] A. Jain, S. P. Ong, G. Hautier, W. Chen, W. D. Richards, S. Dacek, S. Cholia, D. Gunter, D. Skinner, G. Ceder, et al., Commentary: The materials project: A materials genome approach to accelerating materials innovation, *APL materials* 1 (1) (2013).

[87] D. D. Wagman, Nbs tables of chemical thermodynamic properties, *J. Phys. Chem. Ref. Data* 11 (1982).

[88] Y. Chen, S. Fan, G. Gao, Theoretical insights into the defect performance of the wide bandgap semiconductor bas, *Physical Chemistry Chemical Physics* 25 (16) (2023) 11745–11755.

[89] R. Li, A. B. Seddon, Gallium–lanthanum–sulphide glasses: a review of recent crystallisation studies, *Journal of non-crystalline solids* 256 (1999) 17–24.